

THE EFFECT OF THICKNESS AND PLASTIC BEHAVIOR ON THE VALIDITY OF
SUB-SCALE TENSILE TESTING OF TITANIUM

A Thesis

by

LAURA MOODY

Submitted to the Office of Graduate and Professional Studies of
Texas A&M University
in partial fulfillment of the requirements for the degree of

MASTER OF SCIENCE

Chair of Committee, James D. Paramore
Co-Chair of Committee, Ankit Srivastava
Committee Members, Alaa Elwany

Head of Department, Ibrahim Karaman

May 2021

Major Subject: Materials Science and Engineering

Copyright 2021 Laura Moody

ABSTRACT

Today's evolving technological landscape relies increasingly on small-scale components, which puts a premium on small-scale property data. The change in a material's mechanical behavior as the working length scale is reduced is known as the size effect. In this paper, the effect of thickness on the mechanical properties of sub-scale tensile specimens is presented in two materials—Grade 2 and Grade 5 titanium. Thicknesses of 0.2 to 1 mm were tested, while the gauge width and length were held constant at 1 mm and 5 mm, respectively. Unpolished and polished specimens were both tested to understand the effect of surface finish on the properties, principally because Grade 5 titanium (Ti-6Al-4V) is widely known to be notch sensitive. The ultimate tensile strength (UTS) and yield stress (YS) for both materials were not shown to be thickness dependent. However, the total elongation and elongation at UTS showed a linear dependence with thickness according to the p-values of the Pearson's correlation coefficients for the linear relationship, which were less than the chosen significance level of 0.05. The relationship between thickness and elongation is more significant in Grade 2, and this can possibly be explained by its greater necking propensity, which occurs more severely in thinner samples. That is, it necks through the entire thickness quicker in a thin sample than in a thick one. Grade 5 does neck, but it necks to a smaller degree than Grade 2. Therefore, the thickness effect is less pronounced. This investigation showed that thickness as well as the material's inherent plastic response affects ductility. Additionally, two novel cross-sectional area measurement techniques were established to account for material loss due to polishing and to obtain a more accurate area, referred to

as the optical method and the electrical resistance method. These methods are especially useful for instances where micrometers are known to result in significant error (e.g., situations where mass finishing or electro-polishing are used to improve the surface finish of samples). Accurate area measurement is a critical component of sub-scale testing, especially.

DEDICATION

I dedicate this work to my husband, Andrew, whose love, support, and sense of humor kept me going, through it all.

ACKNOWLEDGEMENTS

I would like to thank my committee chair, Dr. Paramore, as well as Dr. Brady Butler and my committee members, Dr. Srivastava and Dr. Elwany for their guidance and support throughout the course of this research.

Thanks also go to my friends and colleagues and the MSEN department faculty and staff for making my time at Texas A&M University a truly memorable and positive experience.

Finally, thanks to my husband for his encouragement and helpful insight into many research-related dilemmas I encountered along the way.

CONTRIBUTORS AND FUNDING SOURCES

Contributors

This work was supervised by a thesis committee consisting of Dr. James Paramore [Primary advisor], Dr. Brady Butler, and Dr. Ankit Srivastava [Co-advisor] of the Department of Materials Science & Engineering and Dr. Alaa Elwany of the Department of Industrial & Systems Engineering.

Much of the data presented in Chapter IV are the result of collaborations with James D. Paramore (ARL/TAMU), Brady G. Butler (ARL/TAMU), Ion J. Powell (TAMU), Daniel O. Lewis (ARL/TAMU), and Matthew C. Johnson (ARL/TAMU).

All other work conducted for the thesis (or) dissertation was completed by the student independently.

Funding Sources

This research was sponsored in part by the Army Research Laboratory and was accomplished under Cooperative Agreement Number W911NF-17-2-0145. The views and conclusions contained in this document are those of the authors and should not be interpreted as representing the official policies, either expressed or implied, of the Army Research Laboratory or the U.S. Government. The U.S. Government is authorized to reproduce and distribute reprints for Government purposes notwithstanding any copyright notation herein.

TABLE OF CONTENTS

	Page
ABSTRACT	ii
DEDICATION	iv
ACKNOWLEDGEMENTS	v
CONTRIBUTORS AND FUNDING SOURCES.....	vi
TABLE OF CONTENTS	vii
LIST OF FIGURES.....	ix
LIST OF TABLES	xii
CHAPTER I INTRODUCTION	1
Background & Technical Relevance.....	1
Problem Statement	1
Hypothesis.....	2
Objectives of this Research.....	3
CHAPTER II LITERATURE REVIEW.....	4
The Size Effect	4
Sub-Scale Testing in Additive Manufacturing (AM).....	5
Sub-Scale Testing in Nuclear Applications	6
Geometrical Considerations for a Sub-scale Tensile Specimen.....	7
Influence of Surface Roughness.....	12
CHAPTER III MATERIALS & METHODOLOGY.....	15
Experimental Design	15
Machining Method	17
Polishing Method	19
Cross-sectional Area Measurement.....	21
Experimental Apparatus & Digital Image Correlation (DIC).....	22
CHAPTER IV AREA MEASUREMENT TECHNIQUES*	25
Background	25
Experimental Procedure	26

Sample Dimensions	26
Optical Method.....	28
Electrical Resistance Method	34
Results	40
Discussion	49
Conclusions	52
CHAPTER V RESULTS & DISCUSSION	54
Roughness Measurements	54
UTS and YS Data.....	55
Thickness-Elongation Relationship.....	57
CHAPTER VI CONCLUSIONS	63
Future Recommendations.....	65
REFERENCES	66
APPENDIX	73

LIST OF FIGURES

	Page
Figure 1: A bowtie-shaped microsample secured in the grips [25].....	7
Figure 2: (a) MT1 specimen (b) MT2 specimen [27]	8
Figure 3: (a) Micro tensile specimen (b) Regular tensile specimen [3].....	10
Figure 4: (a) Build Array of 120 Tensile Specimens. (b) Printed array of 120 Tensile Specimens. (c) Tensile Specimen Geometry [6].	11
Figure 5: Reported Roughness values of Ti-6Al-4V in a Fatigue Study [29].....	13
Figure 6: (a) Grade 2 microstructure showing the typical equiaxed α grains (b) Grade 5 microstructure showing equiaxed α grains with intergranular retained β grains typical of mill annealed material.....	15
Figure 7: Sub-scale tensile specimen shown with symbolic dimensions.....	16
Figure 8: Schematic of wire electrical discharge machining. [34].....	18
Figure 9: A diagram showing the successive stages in the manufacturing process of sub-scale samples.....	18
Figure 10: The LabView interface used for the input of test parameters in tensile testing.....	23
Figure 11: Cropped image of a tensile specimen with the applied speckle pattern.	23
Figure 12: Optical setup: (a) camera and telecentric lens, (b) stepper motor and 2-axis goniometer stage with 3D printed grip and sample gauge, and (c) LED telecentric illumination source. Reprinted from [35].	28
Figure 13: How ImageJ selects an area to threshold. The yellow lines of (a) and (c) are the perimeters of the selections (b) and (d), respectively. (a) A representative miniature tensile bar used in this study, and (c) a NIST certified pin gauge. Reprinted from [35].	32
Figure 14: Plotted from polar coordinates into Cartesian coordinates. Measured: the raw data processed by ImageJ. Rectangular: the simulated rectangle from the two important minima in the measured data set. Calculated: the data set taking the closest points to the origin from both the measured and rectangular data sets. Reprinted from [35].	33

Figure 15: Miniature four-point probe circuit diagram. Reprinted from [35].....	36
Figure 16: (a) Miniature four-point probe setup showing the placement of the current and voltage probes, and (b) perspective view of the same. Reprinted from [35].....	37
Figure 17: Correlation between the areas measured via the optical and resistance methods (ordinate) versus the areas measured using a traditional micrometer (abscissa) for all conditions used in this study. Perfect correlation should produce a linear trend with a slope of 1 and intercept of 0. Reprinted from [35].....	43
Figure 18: Combined plots containing all the sample areas, measured with the (a) optical method and the (b) resistance method. Reprinted from [35].	44
Figure 19: (a) ANSYS model showing probe placement and the location of the current source, and (b) percent of cross-sectional area match as a function of voltage placement. Reprinted from [35].	44
Figure 20: The measured areas for the gauge pins using (a) optical method, and (b) resistance method. Reprinted from [35].	48
Figure 21: Average roughness values as measured across the sample face, for EDM, Part EDM, and AB400Buff.	54
Figure 22: (a)(b) UTS vs. thickness for all sample conditions (c)(d) YS vs. thickness data for all sample conditions. The dotted line represents the benchmark values obtained from certified full-scale tests of ASTM E8 tensile samples. ...	56
Figure 23: Total elongation as a function of thickness for all sample conditions of Grade 2 (a) and Grade 5 (b), respectively. The dotted line represents the total elongation obtained from certified full-scale tests of round ASTM E8 tensile samples.	57
Figure 24: Linear regression performed on the elongation as a function of thickness for (a) Grade 2 and (b) Grade 5 titanium samples.	58
Figure 25: (a)(b) Plastic strain at UTS (e_u) vs. thickness for Grade 2 and Grade 5 titanium, respectively. (c)(d) Post-necking elongation (e_n) vs. thickness for Grade 2 and Grade 5 titanium, respectively.	59
Figure 26: (a) Fracture surface of 1.118 mm thick Grade 2 sub-scale sample (b) Fracture surface of a 1.115 mm thick Grade 5 sub-scale sample.	61

Figure 27: (a) Post-mortem Grade 5 sample, showing minimal necking (b) Post-mortem Grade 2 sample exhibiting significant necking.61

LIST OF TABLES

	Page
Table 1: Roughness Measurement Parameters.....	20
Table 2: Sample Naming Convention.	20
Table 3: Sample Conditions used in this study. Reprinted from [35].	26
Table 4: P-values calculated for the Pearson’s correlation coefficient in each case.	60

CHAPTER I

INTRODUCTION

Background & Technical Relevance

The need for small-scale property data has never been greater. The booming electronics, additive manufacturing, and renewable energy sectors all benefit from small-scale technology. The dwindling size of mechanical components creates a demand for material performance data at increasingly smaller length scales. Micro-electromechanical devices play a pivotal role in the automotive, consumer, industrial, and aerospace industries [1]. In additive manufacturing (AM), small-scale and micro-samples can help unlock the relationship between AM process parameters and the resulting microstructure and properties [2][3]. Small samples also enable the study of location and orientation specific properties in AM components [4], and they can potentially be used for quality control or parametric studies to characterize the mechanical behavior of large batches [5][6]. Such tests are helpful for understanding the effects of various AM process parameters such as the effect of beam intensity on grain growth, in beam-based processes. In the nuclear industry, there are constraints associated with irradiation volumes in many facilities that restrict the size of a test specimen. Small specimen test techniques (SSTT) were developed to study the degradation of irradiated materials in nuclear reactors [7].

Problem Statement

With the dwindling sample size comes a change in mechanical behavior at some critical length scale. This change in mechanical behavior at small length scales is known

as the size effect. The goal of the investigation in this thesis was to understand the role of thickness and material on the mechanical properties of miniature tensile specimens. For the experiments in this paper, wrought Grade 2, commercially pure, (CP-Ti) and Grade 5 (Ti-6Al-4V) titanium sub-scale tensile samples with constant gauge width and length were tensile tested at varying thicknesses from 0.2 to 1 mm. The “Grade” of each material refers to its classification based on chemical composition as outlined in the ASTM B348 Standard Specification for Titanium and Titanium Alloy Bars and Billets [8]. Both unpolished and polished samples were tested to analyze the effect of surface finish on the mechanical performance.

Hypothesis

The hypothesis for the experiments outlined above was that both materials would exhibit a change in mechanical behavior proportional to the reduction in thickness. That is, the elongation was predicted to decrease in both materials, as the thickness was reduced, but the extent to which each material would exhibit this thickness effect was unknown. “Small is stronger” is a well-documented phenomenon that occurs in metal samples with very small dimensions [9][10]. However, the mechanisms documented in such studies are only significant at very small length scales, and the thinnest samples in the current work were > 100 times thicker than those used in the cited work. Therefore, it was hypothesized that the strengths recorded in this study would be representative of bulk samples if the surface finish was sufficient to prevent premature failure due to stress concentrators.

Objectives of this Research

The objective of this research was to:

1. Understand the extent to which the material in question dictates the change in mechanical behavior, namely elongation, due to a reduction in thickness.
2. Use the understanding about material influence on the size effect to guide efforts utilizing sub-scale components in material characterization or everyday applications.

CHAPTER II

LITERATURE REVIEW

The Size Effect

With the dwindling sample size comes a change in stress state, and thus a change in mechanical behavior. Theoretically, the stress state of a sufficiently thick sample is plane strain, while that of sufficiently thin sample is plane-stress [11]. In a simplified model, there are no mixed stress states and there is zero stress normal to the direction of thickness for the plane-stress case. However, the real stress state of a sample is closer to that of a plane-strain-like or plane-stress-like state because it is more of a mixed stress state than either one or the other. The flow stress at the onset of plastic deformation should be lower in the plane-stress state, according to Kals and Eckstein's work with copper-silver and brass alloy sheet that showed the flow stress at both the onset of plastic deformation and at the start of necking becomes lower as thickness is reduced [12]. This phenomenon was attributed to the difference in plastic deformation behavior between surface grains and internal grains in thin samples [13]. In a plane-stress state, there is less resistance to deformation because there is less material to provide constraining forces on the surface. Therefore, the amount of surface grains relative to the total number of grains is shown to have a significant impact on the flow stress at some critical length scale. Thicknesses for that investigation ranged from 0.1 to 1 mm. Besides the flow stress size effect due to miniaturization, the ratio of the grain size to the specimen thickness significantly influences the mechanical behavior of thin metal sheets [14][15].

Zhao et al. varied the sample thickness of coarse-grained copper from 250 μm to 2 mm and found that increasing the thickness lead to an increase in both uniform and post-necking elongation [16]. The gauge length and width were held constant at 1 mm and 2 mm respectively for these experiments. In a separate set of experiments, the gauge length was then varied, from 1 mm to 10 mm, with the thickness and gauge width held constant. The amount of uniform elongation lessened as gauge length was increased. Sergueeva et al. found that varying the gauge length of Ti-6Al-4V sheet from 2 mm to 40 mm at constant gauge width and thickness, resulted in a significant decline in uniform elongation [17]. The thickness and width were kept at 115 μm and 1 mm, respectively. Based on literature, both the gauge length and thickness are shown to significantly affect the elongation at failure of sub-standard size tensile specimens. In small-scale testing, the geometry dependence can possibly be explained by the changing stress state and the increased ratio of defect size to cross-sectional volume [18]. One clear theme from literature is that the deformation mechanisms are based on the length scale of operation, and properties such as elongation are more sensitive to the size effect.

Sub-Scale Testing in Additive Manufacturing (AM)

The world of additive manufacturing (AM) experienced massive growth in recent years. The growth is in large part due to advancement in other areas of technologies such as computers, lasers, and microcontrollers [19]. What began as a convenient and cost-effective way to produce low-resolution prototypes has transformed into an evolving manufacturing technique that can rival some mainstream manufacturing techniques. A 2019 Market Outlook report by Smartech estimated that the AM market grew 24% in

2018 to a total market value of 9.3 billion USD [20]. The lure of AM and its general advantage over conventional subtractive, formative, and joining-based manufacturing is that it creates near-net-shapes (NNS), meaning that parts with complex geometries requiring most of the volume to be machined away can be produced with far less waste. Some materials such as titanium alloys and tool steels are cumbersome to machine [21], and the headache of doing so can be reduced by additively manufacturing the component with most, if not all, functional aspects included. Sectors that specialize in producing complex metal parts out of high-cost materials such as titanium arguably stand to reap the most financial benefits from implementing AM technologies. Still, there is much left to understand about the different AM processes and how they influence the integrity of resulting metal components [22]. Small-scale tensile testing has the potential to unlock the details yet to be discovered about metal additive manufacturing and the relationships between process parameters and the resulting properties.

Sub-Scale Testing in Nuclear Applications

The nuclear industry has long focused on small specimen test techniques (SSTT) to study material responses to irradiation [23][24]. The size of an irradiated specimen is largely limited by volume constraints set by safety standards. The geometries in the small specimen test techniques are expected to (1) be representative of bulk properties, (2) be a reduced volume, (3) lead to highly repeatable test results, (4) be resistant to large flexure/distortion in the test rig, and (5) have a reliable data conversion method from small to standard specimens, if necessary. In addition to being representative of bulk properties and having a reduced volume, the specimen should lead to high

repeatability in subsequent testing results and resist flexure or distortion when mounted in the testing apparatus [7]. Flat specimens are usually proportionally scaled down from their standard sized counterparts for testing. The same principles of the SSTT used in the nuclear industry can guide miniature tensile testing efforts for the application of characterizing AM metals.

Geometrical Considerations for a Sub-scale Tensile Specimen

The geometry of a small-scale sample should be such that the sample does not bend or experience flexure in the grips. This follows one of the tenets in the guidelines of the SSTT of materials irradiation research. A popular sample geometry in small-scale testing is the bowtie shape because it is self-aligning when placed in the grips. This type of sample and the accompanying grips were used in a study by Lavan et al. [25] to study the variation in properties by location in HY-100 plate welds, and are pictured in Figure 1.

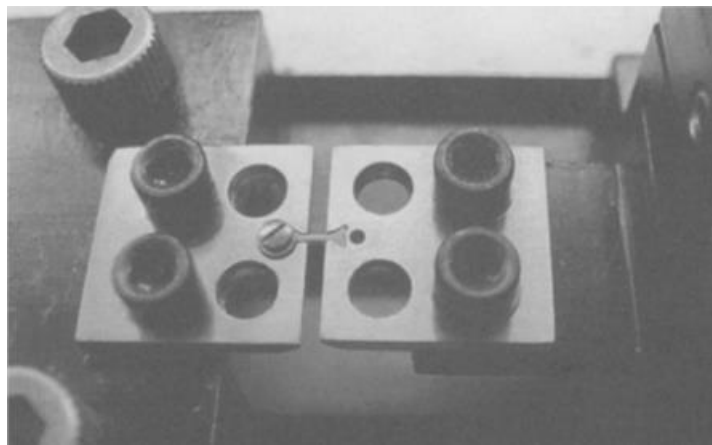


Figure 1: A bowtie-shaped microsample secured in the grips [25].

The microsample test technique was found to yield similar measurements of the elastic modulus (E), yield strength (YS), and ultimate tensile strength (UTS) compared with full-sized samples of HY-100. Typically, a microsample is on or below the length scale of a few millimeters [26]. Therefore, the specimens should be referred to as “miniature” samples instead of “micro” samples to avoid confusion. Karnati et al. [27], used a similar bowtie shaped specimen, along with a second specimen of different geometrical proportions, to study the properties of SLM fabricated 304L stainless steel. Both small-scale specimens with respective dimensions are given in Figure 2.

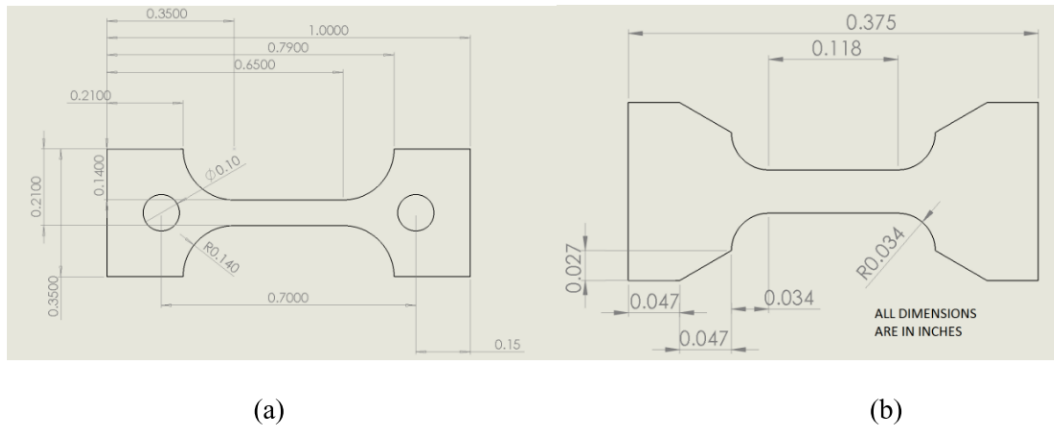


Figure 2: (a) MT1 specimen (b) MT2 specimen [27]

The “MT” abbreviation stands for “mini tensile” sample. The samples were designated as MT1 and MT2 from left to right, according to Figure 2, and each sample was oriented with the tensile axis in the direction of the build. SLM fabricated MT1 and MT2 samples were found to have good agreement on the UTS compared with their wrought counterparts of the same geometry and dimensions. The authors made this determination based on comparing Weibull fits of the UTS data of the bulk and SLM

samples. This may not give an accurate estimation of the property distributions, given that the number of samples tested for each material type ranged anywhere from 35 to 55. However, the wide variation in distribution fits of the YS data between MT1 and MT2 samples might suggest that the material flaw distribution is related to sample size.

An equally popular specimen geometry is one such as the ASTM-E8 sample [28], scaled down. This type of sample was used in a study by Reddy et al. [3] to determine the small scale properties of five different DMLS alloys. Standard cylindrical ASTM E8 specimens were also fabricated via DMLS for the five alloys. Both specimens are shown in Figure 3 with their respective dimensions. Unlike the study by Lavan et. al, the miniature samples were wire EDM cut from the DMLS fabricated blocks. Good agreement was found between the miniature samples and standard samples for YS, UTS, and % elongation for CoCrMo, Maraging steel, and SS316L (<5% difference). IN718 and Ti-6Al-4V micro samples showed less agreement (10% difference), with the properties being lower than the standard samples. However, heat treating the alloys post-fabrication was shown to reduce the property difference to < 2% for all five alloys.

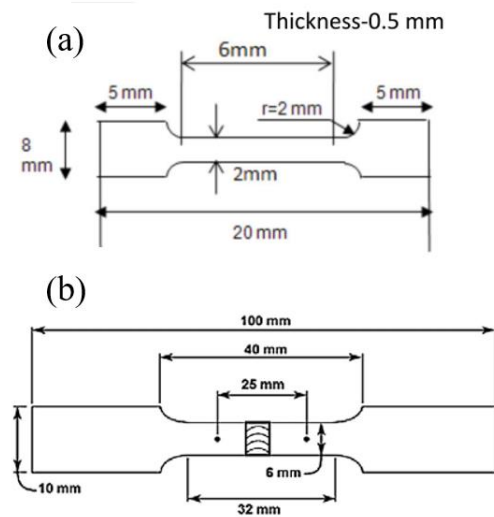


Figure 3: (a) Micro tensile specimen (b) Regular tensile specimen [3].

The study did not include tensile tests of wrought miniature samples. Having such information would have allowed us to compare the miniature and regular sample data and establish that the chosen sample size was in fact appropriate. The miniature tensile sample should be proved to be representative of the wrought bulk properties before it is used to compare wrought and DMLS properties. Additionally, only three samples contributed to the reported average mechanical properties for both specimen sizes. The preliminary results of this study look promising, but more miniature samples should be tested to add weight to the presented conclusions.

Miniature tensile samples are also compelling because they use less material and can potentially provide the same amount of data as a standard sample. This means that vast parametric studies on AM material can be performed at a fraction of the cost of larger samples. Furthermore, small scale samples have the added benefit of taking less time to manufacture. Salzbrenner et al. [6] tested 100 miniature tensile samples to study

the random nature of the mechanical behavior of 17-4PH steel produced via laser powder bed fusion from two different vendors. The sample geometry and printing array are shown in Figure 4. The authors were interested in using the high-throughput method to study how different flaws such as surface roughness and internal lack of fusion porosity affect the statistics of various mechanical properties. The widely popular bowtie shape was used in this study as well.

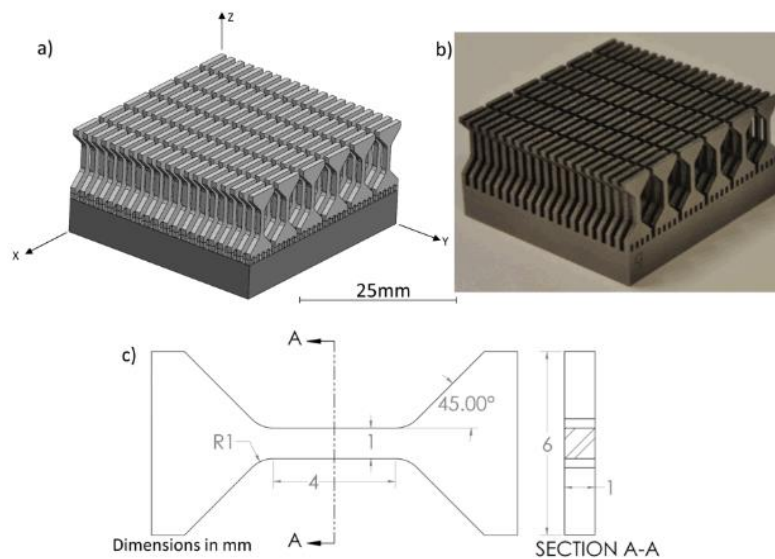


Figure 4: (a) Build Array of 120 Tensile Specimens. (b) Printed array of 120 Tensile Specimens. (c) Tensile Specimen Geometry [6].

While material properties are generally taken to be inherent properties of a material that are scalable, the assumption is that the sample size is representative of the bulk. Whether a sample is a representative element of the bulk can theoretically be determined by principles about the stress state of the sample from mechanics, but the prevalence of defects like surface roughness, microstructural anisotropy, and porosity

are also contributing factors [17]. Therefore, the appropriate tensile specimen size does depend on material characteristics, as well as specimen size and geometry.

Influence of Surface Roughness

Wire electrical discharge machining (EDM) is a popular machining method for titanium alloys, such as Ti-6Al-4V, due to the inherent difficulty of machining these alloys with cutting tools. However, EDM leaves a rough recast layer on every machined surface. Many studies have been conducted on how the surface roughness of the recast layer on the popular titanium alloy, Ti-6Al-4V, effects the fatigue performance of the part. In one study that used three different EDM processes, shown in Figure 5, the difference in fatigue performance was found to directly correlate with the thickness (1-3 μm) and peak-to-valley roughness ($R_{p-v} = 22\text{-}85 \mu\text{m}$) of the recast layers [29]. The fatigue performance was compared with conventionally machined samples of the same material. Both the average roughness, R_a , and the peak-to-valley roughness R_{p-v} were recorded for all specimens, but the R_{p-v} values were more indicative of the types of flaws that initiate fatigue cracks. However, the negative effects of the recast layer were mitigated by post-processing measures such as electrochemical polishing or bead blasting.

Table 2

Roughness of fatigue specimen “test” edges, measured with laser profilometer.

Machining method	Treatment	R_{p-v} (μm)	R_a (μm)
Conventional milling	None	15–30	1.1–1.6
Wire EDM; Shop 1	None	23–41	1.1–1.4
Wire EDM; Shop 2	None	22–33	1.1–1.3
Wire EDM; Shop 3	None	55–85	1.8–2.6
Wire EDM; Shop 3	Chemical Mill	32–63	1.3–1.6
Wire EDM; Shop 3	Electropolish	22–55	0.9–1.3
Wire EDM; Shop 3	Bead Blast	22–26	0.9–1.1

Figure 5: Reported Roughness values of Ti-6Al-4V in a Fatigue Study [29]

Fatigue failure is the result of crack propagation caused by cyclic loading, where the stress concentrates at microscopic flaws which grow into macroscopic cracks of critical size [30]. The degree to which a material is susceptible to fatigue largely depends on the notch-sensitivity of the material. A notch refers to “any discontinuity in shape or nonuniformity in material,” where the stress builds up. The three principal factors affecting notch-sensitivity are: (a) the material capacity to work harden; (b) the degree of material homogeneity; and (c) geometry of the specimen, including the radius of the “root” of the notch being of greatest importance [31].

A fatigue test reveals the dynamic performance of a material, while a tensile test reveals the static performance because the specimen is under quasi-static loading. The focus of this study was the tensile testing of sub-scale titanium specimens and the inherent size effects on the deformation mechanism. It was hypothesized that the main factor affecting the tensile properties would be the scale. However, there was another factor at play. The specimen surface roughness was hypothesized to influence the sample properties, but the extent to which it would contribute was a principal question. Titanium

is known to be a notch sensitive metal, particularly the Ti-6Al-4V alloy more so than commercially pure (CP) titanium, and measures must be taken to reduce the surface roughness for fatigue testing. Unaddressed surface defects are detrimental to the fatigue performance in titanium, especially Ti-6Al-4V. The effect of poor surface finish on a titanium specimen undergoing static loading is arguably less severe yet it remains consequential, especially in the elongation to failure [32]. The extent was hypothesized to depend on the presence and concentration of surface defects.

CHAPTER III

MATERIALS & METHODOLOGY

Experimental Design

The objective of the study was to find the smallest tensile sample size that represented the bulk mechanical properties of the Grade 2 and Grade 5 titanium, while considering the effect of surface roughness on the mechanical properties. Wrought commercially pure titanium (Grade 2) and the industrially favored $\alpha+\beta$ titanium alloy, Ti-6Al-4V (Grade5), were the materials of study. The material certifications for both Grade 5 and Grade 2 from the manufacturer can be found in Appendix A, in **Error! Reference source not found.** and **Error! Reference source not found.**. Micrographs of the microstructures are show in Figure 6 for each material.

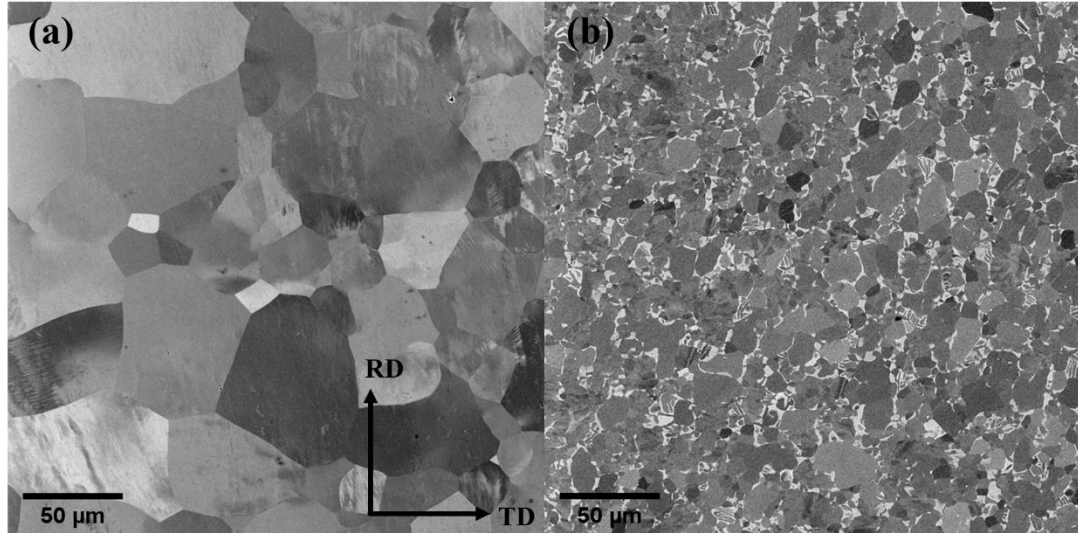


Figure 6: (a) Grade 2 microstructure showing the typical equiaxed α grains (b) Grade 5 microstructure showing equiaxed α grains with intergranular retained β grains typical of mill annealed material.

The Grade 5 micrograph shows subtle elongation in the rolling direction. However, the elongation of the grains is less pronounced than what would be seen in a heavily worked Grade 5 sample. Therefore, there should be less anisotropy in this material than there would be in a heavily worked sample with the same chemical makeup.

A sub-scale tensile sample, with a 1 mm gauge width, was designed to have the same dimensional proportions as an ASTM E-8 flat tensile sample. All dimensions are shown symbolically in Figure 7.

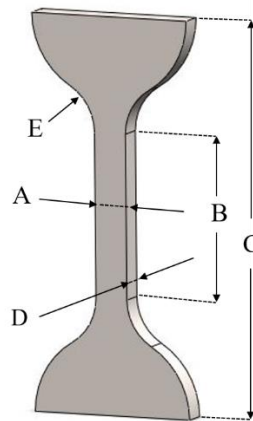


Figure 7: Sub-scale tensile specimen shown with symbolic dimensions.

The thickness of the samples, D, was varied from 0.2-1 mm. The following dimensions refer to those denoted in Figure 7. The gauge length of all tested samples, B, was 5 mm. The gauge width, A, of all tested samples was 1 mm, and the fillet radius, E, was ≥ 1 mm. The overall sample length, C, was 10 mm.

Machining Method

The method for machining the samples was chosen largely with the goal of characterizing additively manufactured titanium in mind. It is likely that metal sub-scale tensile samples would be machined from an AM part by conventional means in a research laboratory using a CNC. However, titanium is notoriously more difficult to machine than most steels or aluminum alloys because it has poor thermal conductivity and does not dissipate heat as well as those aforementioned metals due to its high toughness [33]. Roughly 50% of the generated heat gets conducted into the tool, and the high heat combined with the chemical reactivity of titanium causes the chips to pressure weld readily to the tool, accelerating its wear rate [21]. The challenges of conventionally machining titanium are exacerbated as one attempts to machine a sub-scale tensile specimen using a 1/16" or 1/8" end mill. The small end mills often cannot withstand the machining conditions and break readily and often during the process. Furthermore, the residual machining burrs around the sample edges are jagged and irregular leading to a non-uniform surface finish.

Wire electrical discharge machining (EDM) was found to be a far easier means of machining the miniature samples because it uses a series of electrical discharges between the workpiece and the wire electrode to cut through the material, shown in Figure 8. There is no direct contact between the wire itself and the titanium. Parts with complex geometry can be machined easily using EDM, and it leaves a uniform residual roughness on the sample.

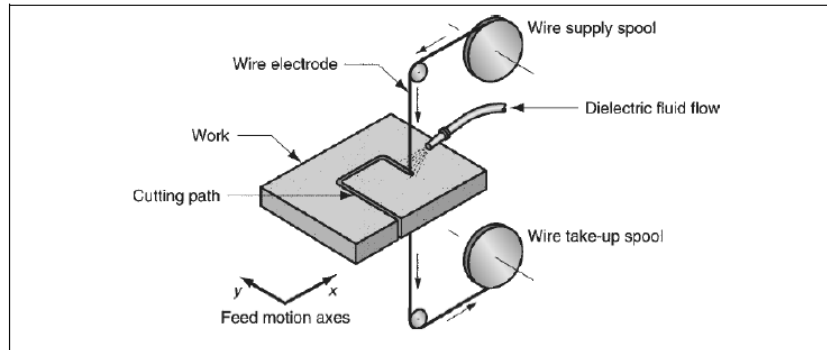


Figure 8: Schematic of wire electrical discharge machining. [34]

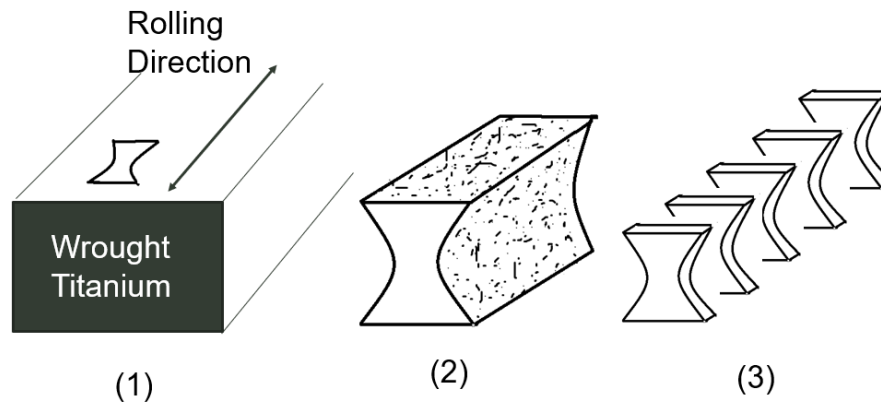


Figure 9: A diagram showing the successive stages in the manufacturing process of sub-scale samples.

The samples were EDM cut from certified wrought bar stock, as shown in graphic (1) of Figure 9. The sample profile was oriented longitudinally with the rolling direction. The result of the EDM step is what resembles a very thick tensile sample. This is shown in graphic (2) of Figure 9, where the speckled surfaces represent an EDM recast layer. After the sample profiles were EDM cut from the wrought material, they were then sectioned with a rubber bonded silicon carbide cut-off blade in a high-speed

metallographic saw (ATM Brillant 220). The individual samples cut from the profile are shown in graphic (3) of Figure 9. The samples were referred to as the “Part EDM” samples, due to the hybrid machining approach. Samples that were both initially cut and sectioned using EDM are referred to as “EDM” samples.

Polishing Method

The partial EDM sample profiles were polished in a series of steps. The first step was grit blasting using AGSCO GMA garnet 36 natural blasting abrasive to remove much of the recast layer. Then, the EDM profiles were secured in a vice, and 400 grit abrasive wheels on a rotary tool were used to smooth all surfaces with the recast layer. Then, cloth wheels were used to polish the samples with a sequence of Porter-Cable cleaning and polishing compounds. A sequence of four compounds were used, starting with a coarse polishing compound, and ending with a fine polishing compound. After the profiles were sectioned, the samples were mounted to an aluminum plate with a wash-away sample adhesive (Crystalbond™) for the next phase of polishing. The cloth wheels and compounds were again employed for the specimen faces, and the abrasive wheels were not used. The samples polished with the combination of abrasive and cloth wheels are referred to as the “abrasive + buff” samples.

Roughness measurements were taken across the samples faces of ten EDM, Part EDM, and “abrasive + buff” (polished) samples using the 3D Roughness Reconstruction software available on a Phenom XL scanning electron microscope (SEM). Table 1 lists the SEM parameters used while taking the measurements, including magnification and waviness filter values. The waviness filters, λ_s and λ_c , are values that are used to

distinguish the roughness of a surface from the larger surface geometry. For these measurements, the roughness profiles were filtered to exclude wavelengths below 20 μm and above 40 μm . The collected values from the roughness measurements are given in Chapter V.

Table 1: Roughness Measurement Parameters.

Material	Magnification	λ_s (μm)	λ_c (μm)	Measurement Length Range (μm)
Grade 5 Titanium	400X	40.0	20.0	600-800

The samples were named according to the type of preparation they underwent.

Table 2 provides each name as well as an explanation for the naming convention.

Table 2: Sample Naming Convention.

Sample Name	Description
PartEDM	Unpolished, as machined
PartEDM-Ground	Unpolished, ground down on one side using either 180 or 320 SiC polishing paper
PartEDM-Buff	Polished using cloth buffing wheels with compound
PartEDM-AB400Buff	Polished using 400 grit abrasive wheels, cloth buffing wheels with compound

As previously mentioned, the initial labeling of “PartEDM” refers to samples that were initially EDM cut and then subsequently sectioned using a precision saw. The

unpolished samples are referred to as “PartEDM”. The name “PartEDM-Ground” denotes samples that were ground down on one side to the desired final thickness using either 180 or 320 grit SiC polishing paper. It was not possible to cut samples to thicknesses of 0.3 mm or less using only the metallographic saw. Instead, the samples had to be cut to 0.4 mm first, and then they were subsequently ground down to achieve the final desired thickness. It was hypothesized that the polished samples would exhibit superior properties compared to those of the unpolished samples due to the removal of surface imperfections that could lead to premature failure. Both type of polished samples, “PartEDM-Buff” and “PartEDM-AB400Buff”, were abrasive blasted prior to polishing.

Cross-sectional Area Measurement

The gauge dimensions of flat tensile specimens are typically measured with micrometers. However, there was some concern about whether polishing the samples would result in significant error in measuring cross-sectional area due to preferential removal of material at the sharp corners of the cross-section, and therefore, rounding the profile. The area of miniature tensile samples is especially affected by material loss from polishing, given that the material loss is a more significant portion of the total area. Two alternative measurement methods were developed as a result, which are referred to as the optical method and the electrical resistance method [35]. The development of these two methods became an important accomplishment in the research and is described at length in Chapter IV.

Experimental Apparatus & Digital Image Correlation (DIC)

The samples were tensile tested on a 1 kN stage at a strain rate of $5 \times 10^{-4} \text{ s}^{-1}$. The bowtie shape of the sample was chosen so the sample could rest easily in the cavity of the self-aligning grips. Samples having a 0.2 mm thickness and below required magnets to hold the sample in place on the grip sections to prevent slippage. Strain was measured using digital image correlation (DIC) with Vic-2D software (Correlated Solutions Inc.). Throughout the test, images were captured at a rate of 0.2 Hz with a FLIR 12 MP Grasshopper high performance USB 3.0 monochrome camera from Point Grey Research, Inc. that was fitted with a variable magnification lens from Edmund Optics and a polarizing filter. The telecentric lens was used to ensure that changes in the working distance of the specimen did not distort the size of sample features. The polarizing filter was used to minimize the amount of light behind the specimen profile. The load cell used was an LCM 300 model load cell from Futek with a 250 lbf (1kN) capacity, and the linear actuator used was from Zaber, model# NA34C60. The stepper motor controller was also from Zaber, from the T-MCA series. A custom LabView code was used to control the input parameters and testing apparatus. Figure 10 shows the graphical user interface (GUI) where inputs such as the sample name, gauge thickness, and width were input. The code also saved the load, stress, displacement, and time data.

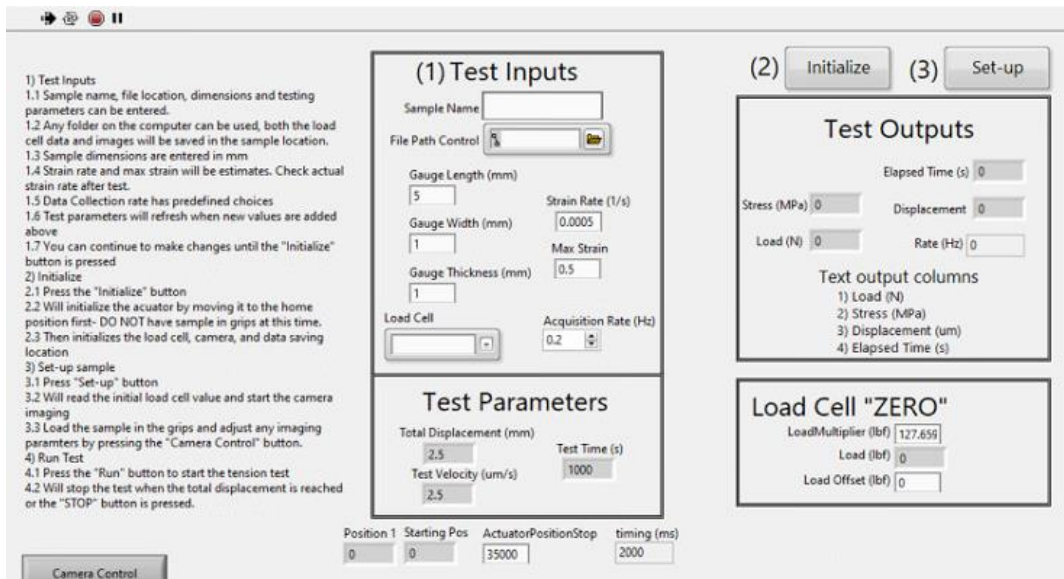


Figure 10: The LabView interface used for the input of test parameters in tensile testing.

The samples were painted with a black and white speckle pattern to ensure that the Vic-2D software was able to measure the strain accurately. An example of the speckled pattern on a sample is shown in Figure 11. The speckle pattern was achieved by mixing water-based white paint with black ink toner in a 20:1 weight ratio. The paint was applied evenly to the samples using a Central Pneumatic airbrush kit at a pressure of 45 psi.

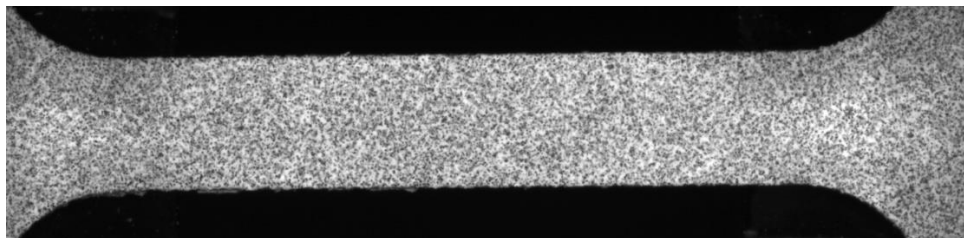


Figure 11: Cropped image of a tensile specimen with the applied speckle pattern.

DIC involves using the sample images to compute surface displacements, and the subset and step size are two dimensions that are critical in these calculations. A rectangular region of interest is first selected for the specimen, extending slightly past the gauge section. The first image in the set is referred to as the reference image. In Vic-2D, the reference image is divided into subsets of the size that Vic-2D determines to be appropriate for the given speckle pattern. The appropriate subset size for most samples was in the range of 60-80 pixels, based on the speckle pattern. The subset is a portion of the pattern chosen for tracking. Unless there is a large amount of deformation in the sample, the same subset in subsequent images is compared to that of the reference image. Then, the relative displacement between the center points of the subsets is computed. The strain is obtained from this value.

In DIC, each subset should contain at least three speckles [36]. Larger subsets lead to better pattern matching because there is more uniqueness in a single subset, but smaller subsets result in less smoothing of the image data. The step size is the distance between subset centers and should be smaller than the subset size as a rule. The step size chosen for these experiments was 7 pixels. Once the strains for each image were calculated, a digital extensometer equaling four times the gauge length in pixels was drawn on the gauge, and the strain data was obtained from this step. The strain data was then exported and combined with the stress data from the LabView program for further data analysis.

CHAPTER IV

AREA MEASUREMENT TECHNIQUES*

Background

Sub-scale tests require precise measurements of relatively small cross-sectional areas, which is cumbersome with traditional techniques. Accurately measuring the dimensions of a tensile sample is critical for material characterization. Additionally, the relative errors of machining and measuring these samples only increases as sample size decreases. Therefore, the sample cross-sectional area must be measured after machining and polishing with the best feasible accuracy to minimize errors in mechanical property calculations. The gauge width and thickness of miniature tensile specimens, especially those with cross-sectional areas of less than 1 mm², are difficult to measure, even with traditional precision instruments. Measuring the gauge width or thickness of the sample at an angle not perfectly perpendicular to the edges can change the value of the measurement by tens of microns. Furthermore, the cross-sectional area losses due to rounding of the sample's edges during polishing becomes significant in miniature samples. The lack of literature regarding measuring the cross-sectional area of small tensile samples was the motivation to produce this work, which explores two methods of measurement. The first method is optical, which utilizes the software ImageJ and a custom Python code to measure the diameter of projected sample silhouettes at

*Reprinted with permission from “Cross-sectional area measurement by optical and electrical resistance methods for subscale mechanical testing of near-net-shape titanium components” by L. C. Moody, I. J. Powell, D. O. Lewis, M. C. Johnson, B. G. Butler, and J. D. Paramore, 2020. *Int. J. Refract. Met. Hard Mater.*, vol. 92, 105265, Copyright 2020 by Elsevier.

successive angles. The second method uses a material’s electrical properties and a miniature four-point-probe setup to measure resistance and calculate the cross-sectional area of a sample.

Experimental Procedure

Sample Dimensions

While the primary impetus for this study is characterization of NNS titanium components, these proof-of-concept experiments were conducted on certified wrought titanium, both Ti-6Al-4V and commercially pure titanium (CP-Ti). Certified wrought material was chosen because the current work is part of a larger study towards the validation of sub-scale mechanical testing for NNS titanium components, and it was decided that certified material provided a more reliable experimental control. The samples were machined from bar stock using a variety of methods. Table 3 shows the material-machining combinations of all the samples that were measured.

Table 3: Sample Conditions used in this study. Reprinted from [35].

Material	Machining Method	Condition
Titanium, Grade 2	Partial EDM	I
Titanium, Grade 2	Traditional (CNC Milled)	II
Titanium, Grade 5	Partial EDM	III
Titanium, Grade 5	Full EDM	IV

It was hypothesized that the machining method could have an influence on the accuracy of the area measurement techniques, since the machining method influences the resulting surface roughness. The two methods used to prepare samples in this study were electrical discharge machining (EDM) and traditional machining. Partial EDM

samples had the cross-section of the tensile specimen first cut from the bulk material using EDM, which was then sectioned into the final sample dimensions with a rubber bonded silicon carbide cut-off blade in a high-speed metallographic saw (ATM Brillant 220). Traditionally machined samples had the cross-section cut from the bulk material with a CNC mill (Tormach PCNC 440) using a 1.59 mm (1/16 in) diameter 4-flute end mill with a TiAlN coating, which when was then sectioned with the Brillant 220. Full EDM samples had both the initial cross-sectional cut and the sectioning operations done with the EDM.

The relative sample dimensions (i.e. relationships between gauge width, gauge length, fillet radius, etc.) used in this study are extrapolated from recommendations for tension test specimens with rectangular cross-sections in ASTM E8-16a [37]. The specimen grips were rounded to minimize bending moments caused by minor misalignments of the miniaturized tensile apparatus. The following dimensions are all nominal and refer to those denoted in Figure 7. The gauge length of all tested samples, B, was 5 mm. The gauge width, A, of all tested samples was 1 mm. The fillet radius, E, was either 1 mm or 2 mm, depending on the machining method used to produce the sample. Only the samples machined using a CNC mill were designed to have a fillet radius of 2 mm for ease of machining. The other specimens were machined via EDM, so the fillets were kept at 1 mm. The overall sample length, C, was 12 mm in the samples with 2 mm fillets and 10 mm for samples with 1 mm fillets. The overall lengths were adjusted based on the proportions of the specimen, which were dictated by the fillet radius. The sample thicknesses, D, ranged from 0.2 mm to 1.0 mm.

Optical Method

Optical methods for determining cross-sectional area are common in the field of biology [38][39]. These older metrology methods are designed to measure non-uniform objects, such as tendons. However, the proposed optical measurement method is designed for objects with a known general shape, so the flat sides of the object can be simulated, which results in a significant reduction in setup and measurement times. A set of projected silhouette images of the sample are taken at incremental angles, these images are then processed into a dataset showing the apparent projected width as a function of angle.

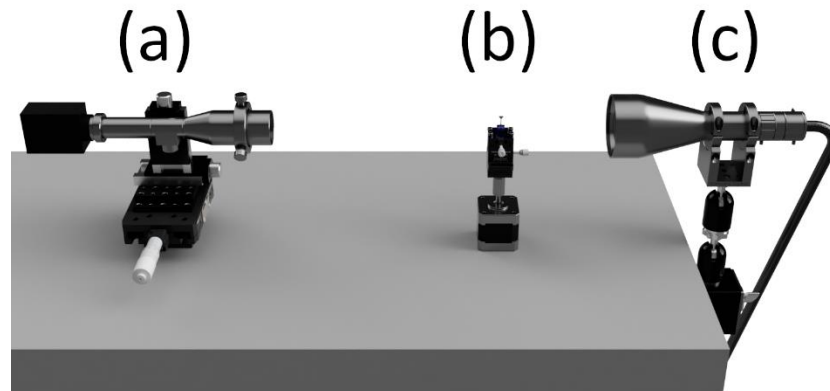


Figure 12: Optical setup: (a) camera and telecentric lens, (b) stepper motor and 2-axis goniometer stage with 3D printed grip and sample gauge, and (c) LED telecentric illumination source. Reprinted from [35].

The setup for the optical method used in this study was minimal, consisting of what is shown in Figure 12. A camera (GS3-U3-120S6M-C) with a telecentric lens (Edmund Optics, In-Line Compact Telecentric Lens 33114) with a linear glass polarizing filter is pointed at the sample gauge with a telecentric illumination source

(Edmund Optics, Telecentric Backlight Illuminator 62760) in the background. The sample is affixed to a 3D printed (Formlabs Form 2) grip with a 2-axis goniometer stage (Thorlabs, GN1/M, GN05/M) for alignment and a stepper motor (NEMA 17HS13-0404S) controlled with an Arduino based CNC controller (UNO Board, CNC Shield V3.0, and A4988 Driver) to orient the sample at specific angles with respect to the camera. Lighting and camera acquisition parameters were chosen to best show the outline of the sample, as shown in Figure 13. A linear glass polarizing filter was oriented to minimize the glare on the sample from other sources of light in the room, which can result in an unclear outline of the sample. Due to the thresholding methods used by ImageJ, blurry images can result in under-approximations of sample areas by artificially diminishing the size of the sample outline used to calculate the area.

The optical measurement system was controlled using a Python program that sent G-code to the Arduino controller and captured images from the camera. The program started by capturing an image and rotating the stepper motor by an incremental angle (1.8° in this case). This procedure was repeated until images for more than half of a revolution had been acquired. This process takes approximately 45 seconds under the current configuration. The Python program relies on having m additional data points on either side of the data set that encompasses the 180° rotation. The number of images, N , that can be used is equal to 180 divided by the incremental angle, θ , plus $2m$, given in equation (1).

$$N = \frac{180^\circ}{\theta} + 2m \quad (1)$$

An important concept in the optical method was the minimum Feret diameter (MinFeret). A Feret diameter is a measurement oriented in a certain direction as the object is enclosed by two parallel planes, similar to a physical measurement with calipers. Each image had its own MinFeret value, which corresponded to the thickness of the projected image of the sample within the yellow lines of Figure 13. The MinFeret value provides the minimum diameter for all possible orientations of two parallel planes. Therefore, since the measurement axis is not fixed, this minimizes the effect of misorientation within the grips. The set of MinFeret values gathered for each incremental angle is the measured data seen in Figure 14. The Feret diameter will artificially inflate the measured cross-sectional area when burrs, protrusions, or debris are present on the surface of the sample as seen in Figure 13(a). However, while this is an important consideration, similar effects are also observed for conventional contact measurements with calipers or micrometers and such defects are easily observed during data acquisition with the optical method.

In order to minimize variations that result from lighting, camera acquisition, and thresholding, a NIST certified pin gauge of known diameter and similar dimension to the sample gauge, as shown in Figure 13(c), was used to calibrate the image scale (pixels/micron) before each series of measurements. An ImageJ script is used to crop the gauge section of the sample, apply thresholds to create a binary (black and white) image, and catalog the shape and size characteristics of the gauge region for each individual image. Thresholds determine the extent of pixels used to create the outlines seen in Figure 13(b) and Figure 13(d) based on how light or dark they are. The threshold applied

to the calibration sample was always kept the same as the thresholding used to find the MinFerret values of the measured sample. After a variety of thresholding values and techniques were tested, the auto thresholding method “Huang”, provided by the FIJI package of plugins for ImageJ, using the thresholding limits of 0 to 33 was found to be optimal.

In order to convert the measured diameter (i.e. MinFerret measurements) to a cross-sectional image in radii, it is necessary to make some basic assumptions about the shape of the cross-section. In this study, the cross section was approximated as a rectangle, ellipse, or some combination thereof. For a purely elliptical sample, the width of the silhouette corresponds to the diameter of the specimen for any given angle. The corresponding radii of this ellipse can be found by dividing the diameter by two. Therefore, it is possible to directly plot the measured values from ImageJ using the MinFerret values and the corresponding angle of the sample when the picture was taken. If the sample is rectangular or rectangular with rounded corners, there will always be two local minima that correspond to the caliper measurements of the thickness and width of the gauge. The MinFerret of each picture of the sample was found and converted to microns using the ratio from the calibration image and written to a .csv file. This file of measured values was input into the cross-sectional area calculation program, which found the important minima. These minima were found when the flat faces of the sample were perpendicular to the camera and light directions, which were used as the length and width of a simulated rectangle, as shown in Figure 14.

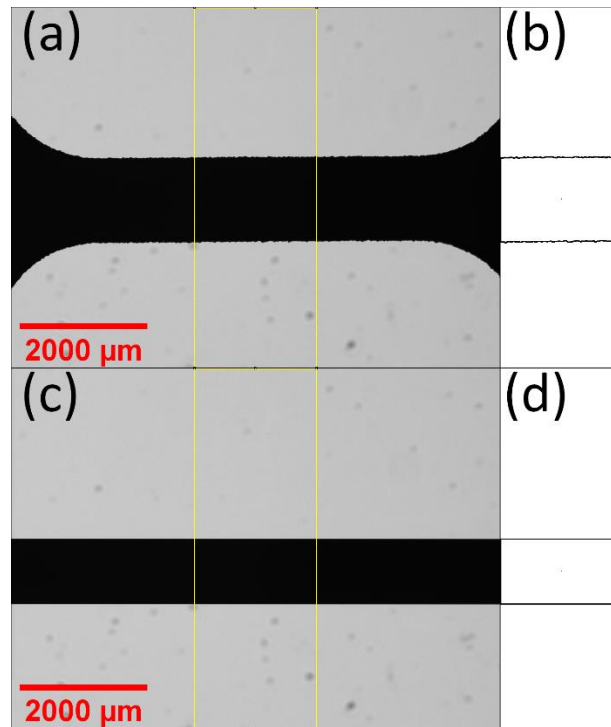


Figure 13: How ImageJ selects an area to threshold. The yellow lines of (a) and (c) are the perimeters of the selections (b) and (d), respectively. (a) A representative miniature tensile bar used in this study, and (c) a NIST certified pin gauge. Reprinted from [35].

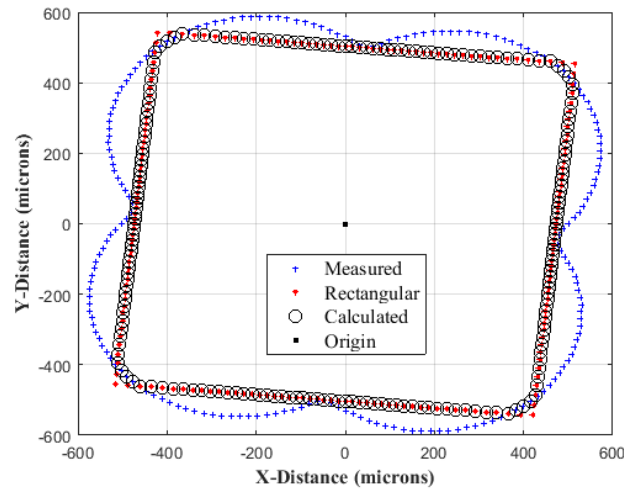


Figure 14: Plotted from polar coordinates into Cartesian coordinates. Measured: the raw data processed by ImageJ. Rectangular: the simulated rectangle from the two important minima in the measured data set. Calculated: the data set taking the closest points to the origin from both the measured and rectangular data sets. Reprinted from [35].

A critical assumption for the construction of the simulated rectangle was that the sides of the sample were perpendicular to each other so that the two important minima from the set of MinFeret values could be representative of the gauge width and thickness. The simulated rectangle shown in Figure 14 was created using the two known important minima, which correspond to the length and width of the rectangle. There were other local minima that were detected from bumps on the sample edge or other inconsistencies with the sample. The Python program sorts through the MinFeret data and determines which minima correspond to the gauge width and thickness. Each MinFeret value spanned the entire sample, meaning each value must be divided by two to plot them as radii. By extrapolating a rectangle using the gauge width and thickness for every point of the measured MinFeret data set, a point was plotted on the rectangle at the same angle.

When the measurements of the MinFerets became smaller than the values from the extrapolated rectangle, it was an indication that those data points corresponded to a rounded corner. These data points are compiled into their own graph which can be used to calculate the cross-sectional area of the sample. A rectangle with rounded corners is the resulting composite image, as shown by “Calculated” in Figure 14, which is taken to be the true cross-sectional profile of the sample. The values in Figure 14 represent 360° of the sample, which was integrated to find the area of the cross-section.

Electrical Resistance Method

One of the advantages of the optical method is that it is non-contact. However, measurements made by the optical method can be largely affected by bumps and burrs on the sample surface and the camera going out of focus for larger samples, due to the narrow depth of field. This problem led the authors to explore another method that utilizes the electrical resistivity of the material. One of the main goals of the measurement study was to create a method that could quickly measure many samples reliably and consistently. The electrical resistance measurement itself is nearly instantaneous. Therefore, it is easy to imagine that a fixture and automated system could be designed to measure cross-sectional areas on very large batches of samples very quickly.

Due to the small resistivity of the materials under investigation, a two-point probe technique would be unfeasible. The contact resistance would be much larger than the bulk resistance, making bulk resistance undetectable. The four-point probe technique manages to avoid this difficulty by using two outer probes for the passage of current

across the sample and two inner probes to measure the potential [39][40]. No current is transferred across the interface between the voltage sense probes and the sample. As such, the contact resistance has no effect on the voltage measurement. Furthermore, if the current source electrodes are sufficiently spaced from the voltage sense probes, the current lines can be assumed to be fully developed and homogenous in the cross-section of the material between the voltage sense probes. Therefore, the four-point technique was used for all electrical resistance measurements detailed in this study.

Pouillet's Law states that, for a given material, the resistance is proportional to the length of the sample and inversely proportional to the cross-sectional area, given that the cross-sectional area is constant along the length and the resistivity of the material is homogeneous [41]. Therefore, if the resistivity of the material is known, the cross-sectional area of the sample can be easily calculated using equation (2).

$$A = \frac{\rho L}{R} = \frac{\rho L I}{V} \quad (2)$$

A is the cross-sectional area of the sample, ρ is the material's resistivity, L is the length between the voltage sense probes, R is the resistance measured between the voltage sense probes (R1 in Figure 15), I is the supplied current, and V is the voltage measured by the sense probes.

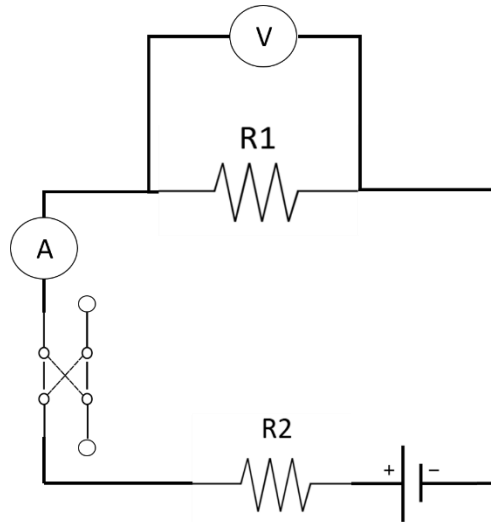


Figure 15: Miniature four-point probe circuit diagram. Reprinted from [35].

The circuit diagram in Figure 15 shows two resistors, R1 and R2. R1 represents the resistance of the sample, while R2 corresponds to a resistor that was added to avoid feeding a current through the circuit that exceeded the maximum 500 mA input of the ammeter. The current source electrodes consisted of two stainless steel screws that could be clamped tightly to the sample and connected to the current source, which was a constant 5V DC power supply. R2 was 18.3Ω (220Ω and 20Ω resistors in parallel). Because R1 was known to be a very small value, the total circuit resistance was approximated to be the same as R2. Therefore, it was calculated that this setup should produce approximately 273 mA through a sample. The actual current was measured with an Extech EX 540 TRMS multi-meter via alligator clips. The voltage sense electrodes were razor blades, which allowed for an extremely thin contact area at each electrode. This maximized the accuracy and precision in determining L in equation (2). Furthermore, razor blades are inexpensive and readily available, thereby enabling

regular changing of the sense electrodes for the best performance. The razor blades were connected to a Keithley 197 auto-ranging microvolt digital multi-meter.

Figure 16 shows the experimental apparatus constructed with both rigid and flexible components. Most of the setup was 3D printed with rigid polylactic acid (PLA), except for the part connected directly to the hinge, which was printed with flexible thermoplastic polyurethane (TPU). Rigidity in the voltage electrode arm was required to keep the blades at a fixed spacing. The flexibility in the hinge component allowed the voltage electrode arm to rotate slightly and accommodate for any small misalignment of the razor blades with the sample surface. This ensured complete contact between the sense electrodes and the sample with minimal applied pressure. Voltage and current measurements for each sample were obtained by lowering the blades onto the sample and applying slight pressure to the top of the blades with an insulating object.

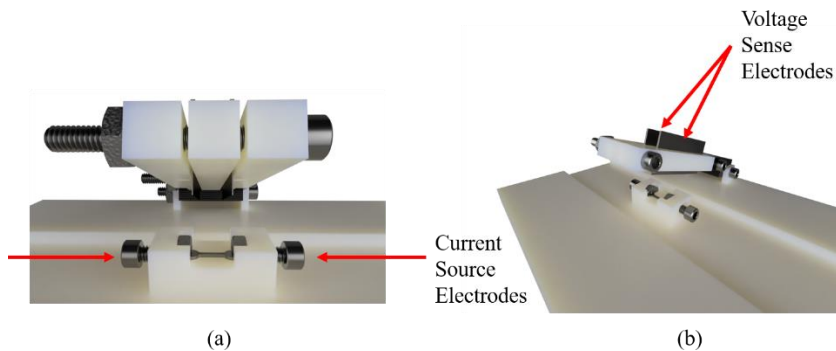


Figure 16: (a) Miniature four-point probe setup showing the placement of the current and voltage probes, and (b) perspective view of the same. Reprinted from [35].

The two razor blades were spaced 7.25 mm apart for 10 mm long samples and 8.15 mm apart for 12 mm long samples. The distances of 7.25 mm and 8.15 mm were chosen so that the blades rested slightly outside the sample gauge section. This means

that while the cross-sectional area was not precisely constant throughout the entire spacing, which is a necessary assumption to use Pouillet's Law, the calculated area was understood to be an average one. An ANSYS model was created to study the effect of probe spacing on the area approximation, which is discussed in the subsequent section. The procedure started with contacting all 4 electrodes to the sample and recording the voltage and current. Then, the switch shown in Figure 15, was flipped to reverse the current for the second set of measurements. The absolute values of the two measurements were then averaged to get one voltage value and one current value for each sample, from which the resistance was determined via Ohm's law. The two measurements were required because of the Seebeck effect, also known as the thermoelectric effect, produced at the dissimilar metal junctions in the apparatus [42]. Most of the measured voltages were on the order of a few millivolts, meaning that several microvolts from the thermoelectric effect could cause a significant error in the area calculations. This effect would be additive to the measured voltage when the current was supplied in one direction, and subtractive by the same amount when the current was reversed. Therefore, an average of the absolute values would yield the actual voltage drop and, therefore, resistance value without any error from the Seebeck effect.

As mentioned previously, the materials used in this study were certified Grade 2 and Grade 5 titanium. However, the accompanying certifications did not specify the electrical resistivities. While resistivity values are available in the literature for all alloys used in this study, it was known that the resistivity of a specific batch of material will depend on its chemistry and microstructure. The manufacturer, for example, can control

the presence of impurity elements which effect the electrical properties. Impurity elements, such as oxygen, increase the resistivity of titanium as the content increases[43]. Therefore, the degree to which the manufacturer monitors and attempts to mitigate the presence of impurity elements in the material can cause slight variations from one batch to another. The resistivity also varies from one polycrystalline metal to another of the same purity because the conduction throughout the material depends largely on the orientation of neighboring grains [44]. The above reasons compelled the authors to obtain experimental resistivity values for the Grade 2 and Grade 5 titanium used in this study.

Using the 4-point probe method, Ohm's Law, and Pouillet's Law, a resistivity value was measured for each material type from samples of known cross-sectional area, which had been carefully determined using a micrometer. The individual resistivity measurements for each alloy were then averaged and found to be within 1% of the published literature values. These experimentally determined values were used in all subsequent cross-sectional area measurements.

It should be noted that the same apparatus used to measure cross-sectional area from resistance was used to measure resistivity from cross-sectional area. Furthermore, this apparatus was designed for the small tensile bars, which were the primary object of this investigation. As such, the samples of known cross-sectional area were limited in dimension, which also limited possible accuracy in measuring their size. Accuracy in determining actual resistivity could be improved by utilizing a larger four-point probe apparatus to measure the resistivity from larger samples. This would improve the

experimental resistivity measurements, thereby improving subsequent cross-sectional area measurements of small samples of unknown size. Therefore, the authors recommend this improvement for future work with this process.

Results

Figure 17 shows the measurements made for all tensile bar samples in this study, which were categorized by condition and measurement method. The ordinate of each plot is the area measured by either the optical or resistance methods developed in this study, and the abscissa is the area measured by the traditional micrometer method. A linear regression is provided on most plots as well, which provides the means to measure the correlation between the alternative and traditional methods (slope and intercept) as well as the scatter in the data (coefficient of determination or R² value). By these analyses, a perfect correlation for a data set between the traditional and alternative methods should produce a slope of unity and an intercept of zero, and perfect consistency should produce an R² value of unity.

The slope values for conditions I, II, and III indicate a close, almost 1:1, relationship between the areas measured through traditional and alternative means. Therefore, these data indicate a strong correlation between the measurements provided by the proposed methods and those produced by traditional means. The intercepts are all nearly zero as well. A positive deviation of the intercept from zero would seem to indicate a propensity for the method to overestimate area, while a negative deviation would seem to indicate an underestimation versus traditional methods. However, the small deviations of the intercept from zero are not consistently positive or negative for

either method. Therefore, the intercept values are likely the result of small stochastic experimental error and the relatively small sample sizes, rather than systematic error in the measurements. A linear regression was not fitted to the plots of condition IV. The range of sample sizes tested for this condition was very small (1.10-1.13 mm²). Therefore, a linear trend line for these data has little statistical significance. If the origin is considered in the data set, by assuming that the alternative methods must physically return an area of zero when no sample is present, a trend line with slope of very nearly unity and an intercept of very nearly zero is produced. This is also supported by the combined plots, discussed in the following paragraph. However, this manipulation of the linear fit was considered unnecessary and possibly deceptive in this analysis.

The plots in Figure 18 show all data produced by either method on the same plot. These combined plots also show strong correlation between the traditional and alternative methods. The slopes and R^2 values of both the optical and resistance methods are close to unity (four are greater than 0.99, and the remaining two are greater than 0.96 and 0.98, respectively).

As shown in Figure 17, the traditionally machined samples (condition II) produced the poorest correlation as well as the poorest linear fit among the conditions. EDM leaves a rough recast layer, but the roughness is more uniform than the condition II samples and has fewer large protrusions. The burrs on condition II samples interfered with the optical measurement accuracy because the outline of the sample became less well-defined and thus more difficult to measure in ImageJ. Additionally, as with the virtual caliper measurement done by ImageJ, these burrs also effect the physical caliper

measurements used as the control in this study. This is evidenced by the data point corresponding to the smallest sample measured by the resistance method, where the area measured by the alternative method was considerably lower than that measured by the traditional method. A large burr on the surface will prevent the micrometer from fully closing, causing the traditional method to overestimate the cross-sectional area of the tensile bar. However, the error caused by burrs on the surface should be mostly eliminated in a typical mechanical characterization study of titanium alloys, for which these methods are proposed. Removal of surface imperfections via polishing or finishing is already a requirement for measuring reliable mechanical properties of titanium alloys.

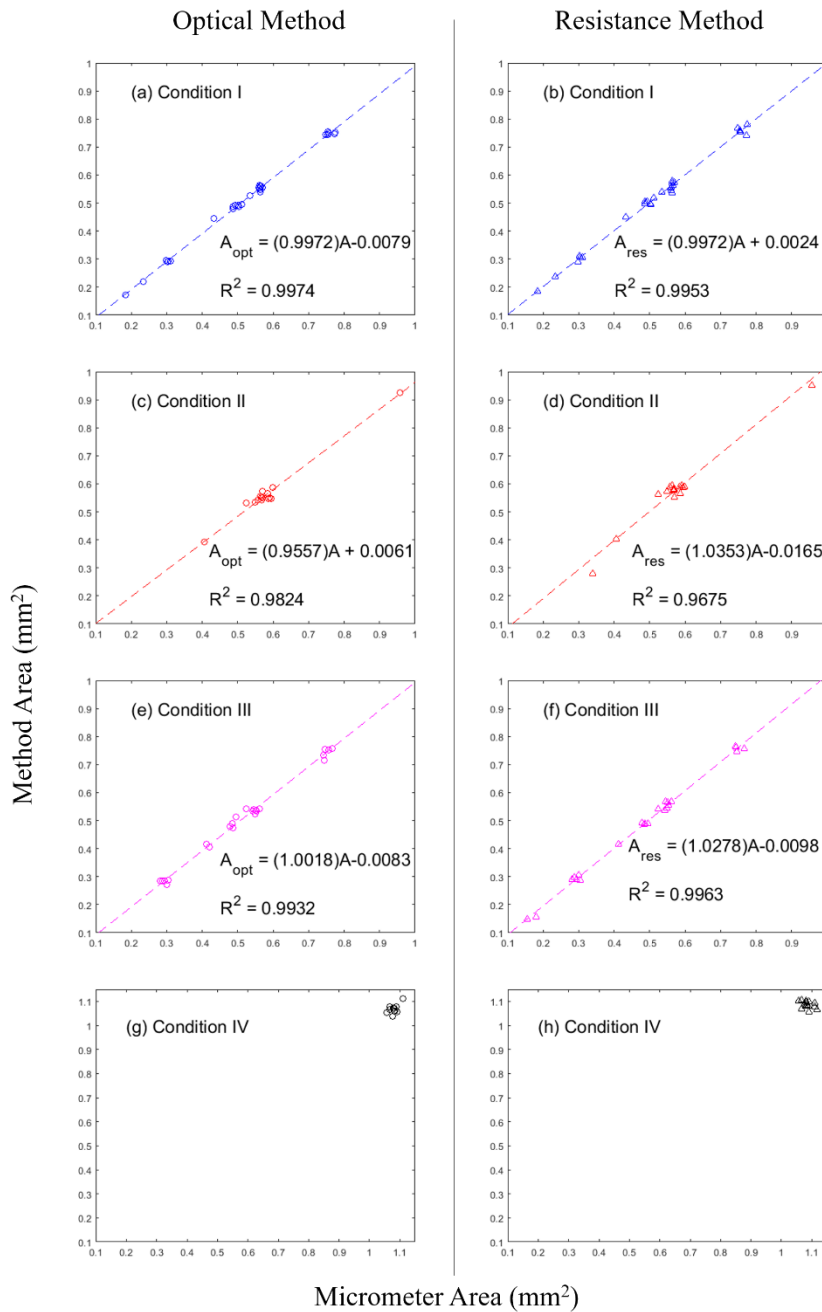


Figure 17: Correlation between the areas measured via the optical and resistance methods (ordinate) versus the areas measured using a traditional micrometer (abscissa) for all conditions used in this study. Perfect correlation should produce a linear trend with a slope of 1 and intercept of 0. Reprinted from [35].

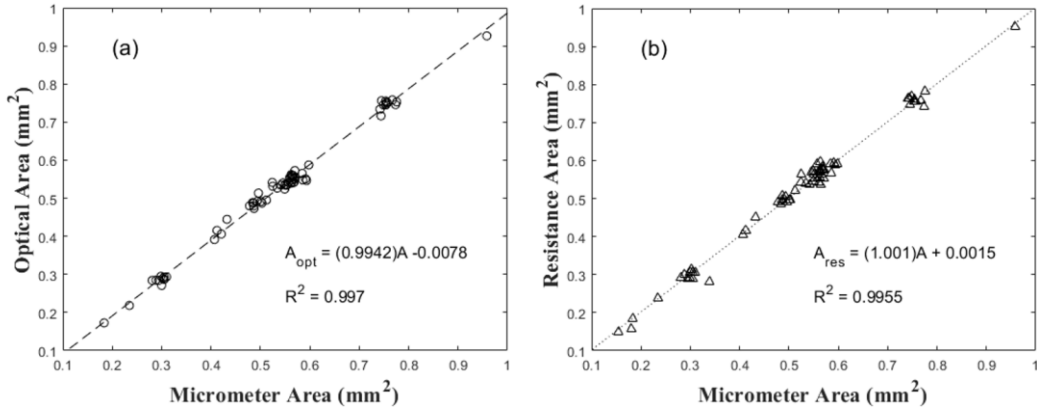


Figure 18: Combined plots containing all the sample areas, measured with the (a) optical method and the (b) resistance method. Reprinted from [35].

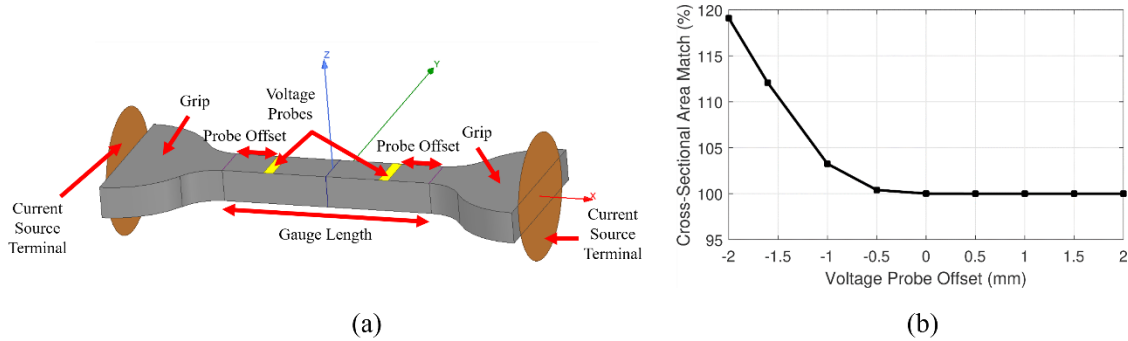


Figure 19: (a) ANSYS model showing probe placement and the location of the current source, and (b) percent of cross-sectional area match as a function of voltage placement. Reprinted from [35].

As mentioned previously, reliably studying the mechanical properties of titanium alloys requires surface finishing after machining to reduce the effect of stress concentrators at the surface. Furthermore, any measurement of a sample's cross-sectional area should be done after polishing to account for any material losses and changes to the part geometry (i.e., rounding of the edges). Therefore, it is desirable to place the voltage sense probes (i.e., razor blades) outside the gauge of the sample to prevent scratching the freshly polished surface. However, a primary assumption in

equation (2) is that the cross-sectional area is consistent between the voltage sense probes. As such, placing the probes outside the gauge is likely to produce a small error in the measurement.

Finite element analysis (FEA) using ANSYS was conducted on the tensile bar geometry to investigate the error due to probe placement. Figure 19 shows a diagram of the analyzed part, indicating the location of the current sources and voltage probes on the sample. The resistivity used in this simulation was calculated from a bulk value of conductivity for commercially pure titanium, found in the ANSYS Maxwell material library to be 1.82×10^6 S/m. As mentioned for the experimental work, it is desirable to use an experimentally determined value due to slight variations in resistivity for the same nominal alloy. However, the purpose of the modelling work was to evaluate relative error based on probe placement. Furthermore, the experimentally determined resistivity for each material used in this study was found to be within 1% of the literature values. And finally, the other values used in these calculations (sample dimensions) were also assumed nominal rather than measured values. As such, the literature value for resistivity was deemed sufficient for this computational analysis.

Several simulations were conducted with varying probe offsets to determine the effect of probe placement on the accuracy of area measurement. An offset of zero indicates that the probes lie directly at the boundary between the gauge and fillet, whereas negative values indicate probe placement outside the gauge section. The error is described by the cross-sectional area match (%), where a value greater than 100% indicates an over approximation of the area. The gauge is the section with the smallest

cross-sectional area, so it follows that placing probes outside of it will result in a larger approximated area. The plot in Figure 19(b) shows the degree by which the area will be overestimated based on how far each probe is from the gauge/fillet boundary.

The ANSYS model was made with property values from Grade 2 titanium, but the trend of the cross-sectional area match applies to Grade 5 titanium samples as well, geometry being the same. Using Figure 19, the percent cross-sectional area match can be calculated for a given probe spacing. The voltage probe offset corresponding to a spacing of 7.25 mm when the gauge is 5 mm long is -1.125 mm, which results in a 105.5% area match. This value, which corresponds to an over approximation of the area by 5.5%, was obtained by interpolation of the data in Figure 19 (b).

The two spacings used in these experiments were 7.25 mm (conditions I, III, and IV) and 8.15 mm (condition II). However, the computational model assumed a fillet diameter of 1 mm, which was only true for samples that had a 7.25 mm probe spacing. Therefore, since the samples analyzed with a probe spacing of 8.15 mm had a different fillet size, the change in cross-sectional area with respect to probe offset was different than the model, making a comparison of condition II data with the model invalid. As previously mentioned in section 3, condition II samples were designed to have a larger fillet radius and overall length for ease of machining with a CNC mill. It was initially thought that the gauge length of condition II samples was longer than 5 mm because of the enlarged dimensions. However, it should be mentioned that this was not the case. Rather, the fillet diameter did not affect the gauge length, which was 5 mm for all

conditions in this study. This user error was the reason that an 8.15 mm spacing was used rather than a 7.25 mm spacing for condition II samples.

The FEA model predicts that the electrical resistance method should overestimate the cross-sectional area by several percent more than that shown in Figure 17, assuming that the traditionally measured cross-sections are perfectly accurate. Based on the slopes in Figure 17, the resistance model had a slope of 0.997 for condition I, indicating an average underestimation of 0.3%, where the model predicted an overestimation of 5.5%. Additionally, the slopes in Figure 17 are 1.028 for condition III, corresponding to an overestimation of 2.8% versus 5.5% predicted by the model.

Due to the uncertainty of measuring the cross-sectional area with micrometers, gauge pins certified by NIST with a known diameter and a tolerance of $+0/-0.0025$ mm ($+0/-0.0001$ in) were also measured with the optical and resistance methods. Having an accurate baseline for the sample area helped the authors get closer to determining the actual error involved in each method. The Class Z pin gauges were produced by the Meyer Gage Company with the material listed as 52100 bearing steel. Only gauge pins having an area equal to or less than the largest tensile sample area (1.12 mm^2) were tested. This was done to ensure that the data sets testing the gauge pins and the tensile samples could be compared on the same scale. An average resistivity value was calculated for the chosen set of gauge pins by using their precisely reported NIST diameters to compute their areas and applying equation (2) to back-calculate resistivity values for each one. The average resistivity value that was used to calculate the experimental areas was $(3.219 \pm 0.043) \times 10^{-5} \text{ } \Omega\text{-cm}$. A voltage probe spacing of

8.15 mm was used. However, the pins had a consistent cross-section along their entire length, meaning the error produced by voltage probe placement on the tensile bars did not apply to the gauge pins. The areas measured using the resistance and optical methods of the pins are shown in Figure 20.

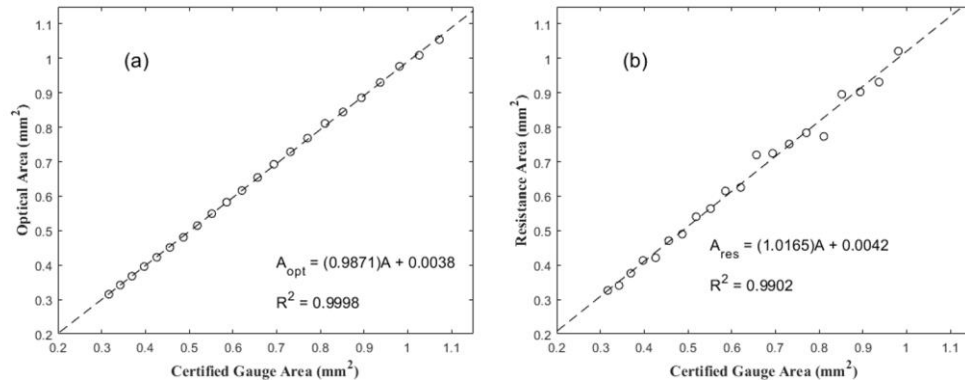


Figure 20: The measured areas for the gauge pins using (a) optical method, and (b) resistance method. Reprinted from [35].

The slope and coefficient of determination of the linear regressions for both methods when used to measure the pin gauge areas against their certified gauge areas are near unity. The slope and R^2 value of the optical method were 0.9871 and 0.9998, respectively, while the slope and R^2 values of the resistance method were 1.0165 and 0.9902. Therefore, when the uncertainty of measuring the cross-section via the traditional method is removed by substituting certified products, both methods appear to be reliable within 1–2% of the actual area. Furthermore, these processes have only been under development for a short time, and it is anticipated that the accuracy and precision of these methods can be increased through optimization and design improvements of the apparatuses.

Discussion

Using miniature tensile samples provides significant benefits for characterizing titanium components produced by near-net-shape processes, such as additive manufacturing and powder metallurgy. Sub-scale tensile samples allow direction- and location-specific properties to be investigated, while reducing the amount of material required for testing. The cross-sectional sample areas studied in this paper ranged from 0.184-1.12 mm². Measuring cross-sectional areas at this scale is an inherent limitation of the traditional method of using micrometer screw gauges, such as the decreased accuracy and increased time consumption involved with measuring many samples. This spurred the authors to develop two new methods for measuring miniature tensile bars with speed and accuracy, which were referred to as the optical method and the resistance method. Both methods were shown to produce area measurements consistent with those obtained with micrometers.

The two methods are fast and easily repeatable for hundreds of samples. The optical setup requires a few basic physical components, along with Python and ImageJ, which are easily accessible programs. As such, both systems were designed to be easy to use and free to access for those who work with miniaturized mechanical testing. Regarding the resistance method, the components were easily produced with parts from a hardware store and a 3D printer, along with basic electrical equipment. Using razor blades as the electrical probes can potentially scratch the sample in the gauge section, which can be a significant issue when testing notch-sensitive titanium alloys. Potential surface defects inside the gauge that act as stress concentrators can be avoided by

placing the probes outside the gauge section towards the grips. The initial area obtained in this manner would be an over-approximation, but a correction factor can be applied to approximate the true area using the chart in Figure 19(b).

The optical method had difficulty dealing with certain factors, namely thickness and surface roughness. The residual burrs leftover from CNC machining increased the surface roughness around the edges, making the outline harder to distinguish and leading to an over-approximation of area using this method. However, the recast layer from EDM and the burrs from traditional machining both caused difficulties measuring the sample areas with the micrometer as well. Poor surface finish is known to be problematic in mechanical testing of titanium alloys. Therefore, these surface defects should be largely eliminated with polishing and finishing techniques prior to measurement and mechanical testing of specimens.

It is the authors' opinion that the electrical resistance method could be optimized to provide a means to very rapidly measure the precise cross-sectional areas of thousands of miniature tensile bars, which could be a valuable resource in studies on large parameter spaces. This opinion stems from the fact that the resistance method measurements are essentially instantaneous. If the other test parameters can be tightly and consistently controlled and the sources of error addressed (i.e. probe spacing, material resistivity), the cross-sectional area of a sample can be directly calculated from the measured voltage and current. As such, it could be imagined that an automated 4-point probe fixture could be used, and the rapidity of the test would be limited solely by

the speed at which sample could be loaded into this fixture. However, there are several considerations that need to be addressed with this process.

As detailed in the previous section, the experimentally determined error based on a comparison of the resistance method measurements with the traditional measurements differed from the computationally modeled error by up to 5.8% of the measured value. However, the model only considered probe spacing as a source of discrepancy between these two methods. Therefore, there are some pitfalls in this comparison. First, the traditional method, as detailed above, is prone to overestimate the cross-sectional area, particularly when surface protrusions exist. If the baseline for comparison is prone to error itself, it confounds the results from the new method. Furthermore, the EDM process used to prepare conditions I, III, and IV produces a recast layer containing brass, which has much lower resistivity than the titanium substrate and may affect the measured resistance in a non-negligible manner. As such, there is likely a combined effect of experimental error in the traditional measurements, in addition to error not solely attributed to probe spacing in the resistance method.

For either method, the most reliable results stem from the analyses of the certified pin gauges. These materials were ground by the manufacturer and certified by NIST standards to a defined tolerance in diameter. Therefore, the primary source of error in the baseline/control used for both methods (micrometer measurements), as well as the primary source of error in the optical measurements, was assumedly ameliorated. If the slope and intercepts of the linear fits are taken to be applicable to experimental studies, either method would produce cross-sectional area data for tensile bars within ~2% of

actual when averaged among all samples of a statistical sample. For Ti-6Al-4V with an ultimate tensile strength of 1000 MPa, this corresponds to an uncertainty of ~20 MPa in the averaged measurements. While the slope and intercept of the resistance method data for the pin gauge samples were close to those of the optical method, there was a significant difference in the regression coefficient. As such, this method is more prone to scatter, which may affect the reliability of measurements, particularly among smaller sample sizes.

Conclusions

Based on the nearly 1:1 measured area correlation given by the slopes in Figure 8 and the small degree of variance, both the optical and resistance measurement methods show promise for measuring the cross-sectional area at the presented scale. While both methods showed small deviation from expected or known values and relatively little scatter in the data, the optical method displayed a slight advantage over the resistance method in this study. However, there are important considerations with either method.

In regard to the optical method, samples with areas above ~1 mm² sometimes extended beyond the camera's depth of field and became defocused during measurement. Therefore, in its current setup, the optical method is best suited for samples with cross-sectional areas below 1 mm². However, this can be overcome for larger samples by modifying the depth of field during acquisition. Therefore, the optical method has proven to be reliable and effective in the laboratory, and it is currently being utilized and further optimized by the authors in mechanical characterization of NNS titanium alloys.

The resistance method could be optimized to provide a means to very rapidly measure the precise average cross-sectional areas of thousands of miniature tensile bars, if the considerations regarding material homogeneity and probe spacing are properly addressed. It is imperative that the material has a homogeneous and well-defined resistivity, which may be difficult to achieve in many additive manufacturing processes that produce inhomogeneous chemistries and microstructures. Furthermore, there is a possibility for significant error if the voltage sense probe spacing is not tightly controlled and accounted for in the data analysis. Therefore, in the authors' opinion, the optical method currently has several advantages over the resistance method, because it is contact-free and the accuracy does not depend on the microstructure or chemistry of the material.

CHAPTER V

RESULTS & DISCUSSION

Roughness Measurements

Measurements were taken across the sample faces of ten EDM, Part EDM and AB400Buff (polished) samples using the 3D Roughness Reconstruction software available with the Phenom XL SEM. Five measurements were taken at three locations across the gauge, yielding a total of 150 measurements per sample set. Only Grade 5 samples were measured because those were the only samples for which surface roughness was of significant interest. Table 1 lists the SEM parameters used to take the measurements, and Figure 21 shows the collected data.

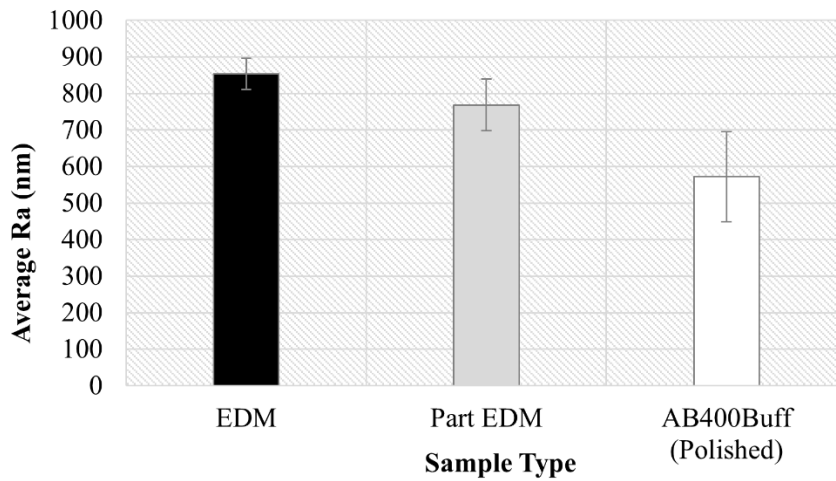


Figure 21: Average roughness values as measured across the sample face, for EDM, Part EDM, and AB400Buff.

Polishing the samples with the abrasive + buff method did result in an average reduction in roughness. However, the standard deviation increased, which was likely due

to the nature of the polishing method. Using a hand-held rotary tool to polish has its drawbacks, namely that the applied pressure is variable, and the surface finish will vary accordingly. The data from Figure 21 suggests that while our polishing method was successful at achieving lower Ra values, those values were not seen consistently over the sample surface. A polishing method that can yield a uniformly smooth surface would ideally replace this method.

Another series of samples were polished exclusively with the cloth wheels and compounds to determine if the abrasive wheel step was unnecessary. The samples prepared with this method were referred to as the “buff” samples. However, the buff method was found to be insufficient at reducing the roughness on all surfaces of the sample. The edges had residual roughness from the recast layer even after grit blasting, and the rough edges translated to poor cross-sectional area measurement using the optical measurement method (Chapter IV). The image analysis code was not able to approximate the area on most of the samples because the bumps were too large. Therefore, polishing with the abrasive wheels was a necessary step to ensure smooth edges.

UTS and YS Data

Mechanical property data was plotted as a function of thickness to discern emerging relationships between the properties and specimen thickness. In total, counting

both unpolished and polished samples, 40 samples were tested for each material. Figure 22 shows the relationship between thickness and both UTS and YS for the materials.

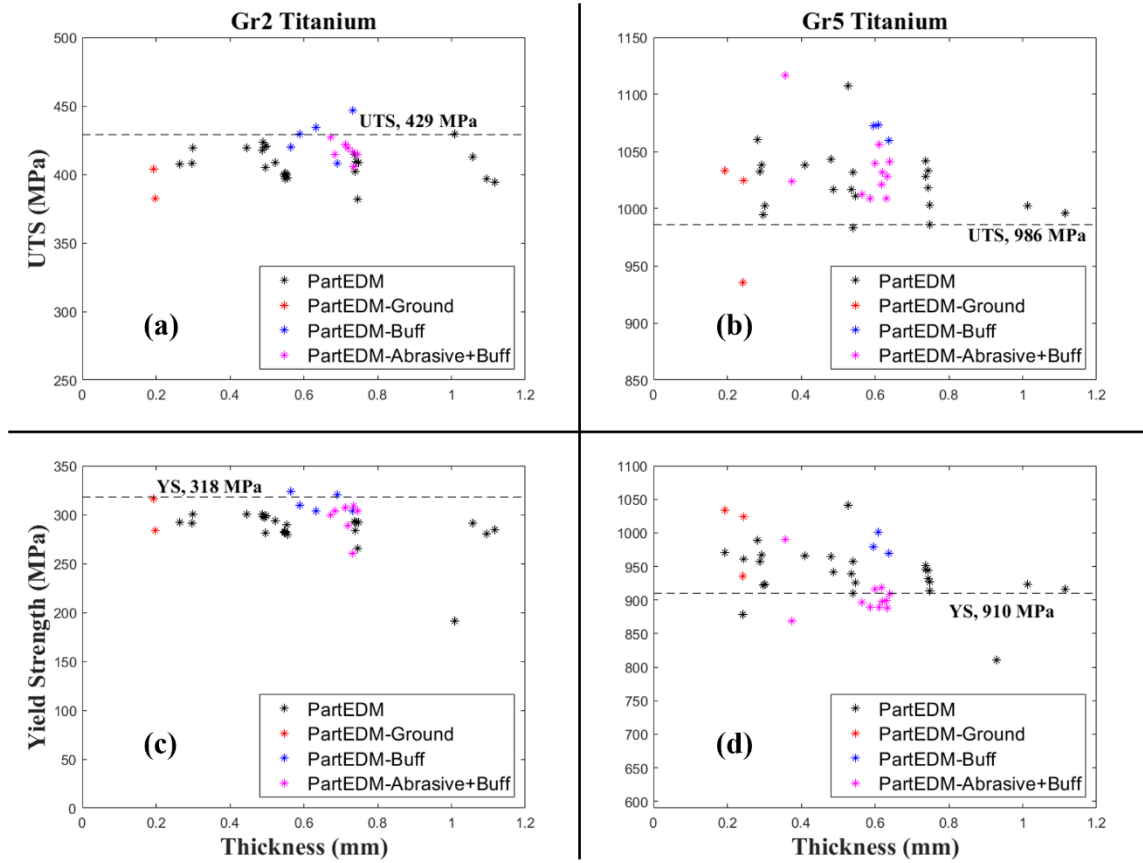


Figure 22: (a)(b) UTS vs. thickness for all sample conditions (c)(d) YS vs. thickness data for all sample conditions. The dotted line represents the benchmark values obtained from certified full-scale tests of ASTM E8 tensile samples.

The polished sample data is consistent with the unpolished data in Figure 22. That is, the polished sample data does not differ considerably for either Grade 2 or Grade 5. There is also a significant amount of scatter in the UTS and YS data for both materials, but it is apparent that most Grade 5 samples have UTS and YS values above

the benchmarks for most thicknesses. Grade 2 sub-scale samples exhibit UTS and YS values either equal to or consistently below the benchmarks, with few exceptions. Based on this data, there is little evidence to suggest that UTS or YS are correlated to the specimen thickness for this range of thicknesses (0.2-1 mm) in either type of titanium. However, it is difficult to say definitively due to the large amount of scatter. Interestingly, once the total elongation was graphed as a function of thickness, signs of a trend between elongation and thickness became distinguishable for Grade 2. The total elongation data is shown in Figure 23 with benchmark values for comparison.

Thickness-Elongation Relationship

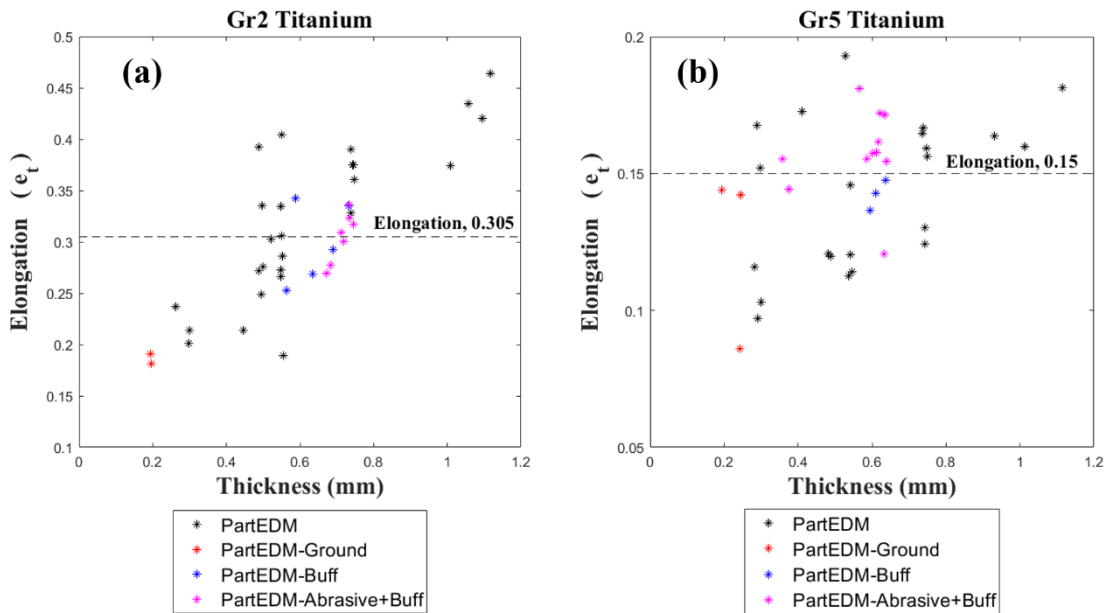


Figure 23: Total elongation as a function of thickness for all sample conditions of Grade 2 (a) and Grade 5 (b), respectively. The dotted line represents the total elongation obtained from certified full-scale tests of round ASTM E8 tensile samples.

Comparing the total elongation data in Figure 23 (a) and (b), there is more of an apparent trend between elongation and thickness for Grade 2 titanium. Therefore, a linear regression was performed for each data set to compare the quality of fit of a linear trend in both materials. The regression coefficients and coefficient of determination, R^2 , were calculated for the linear fit, which is shown in Figure 24. The R^2 value is the square of the correlation coefficient, R , in this case.

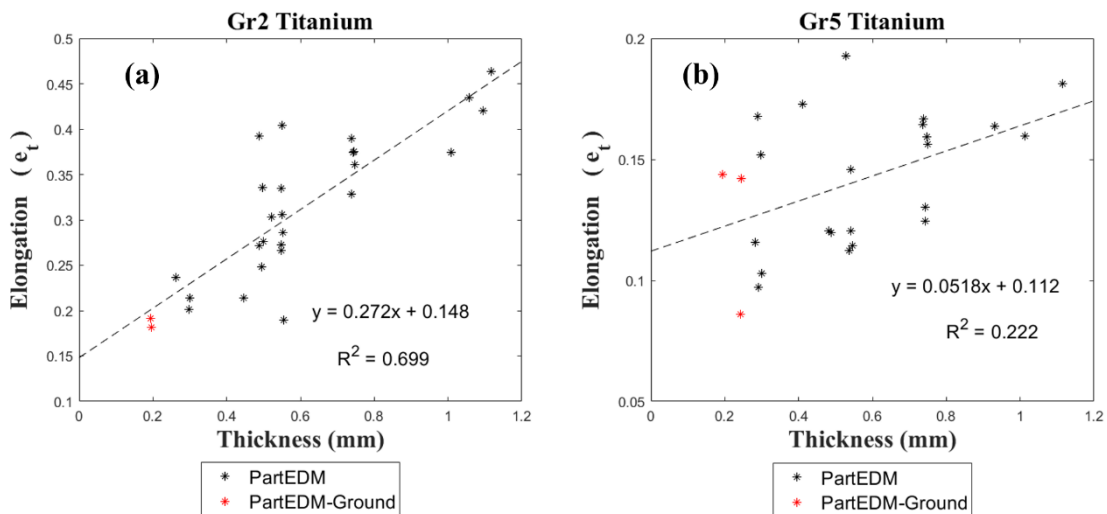


Figure 24: Linear regression performed on the elongation as a function of thickness for (a) Grade 2 and (b) Grade 5 titanium samples.

Polished sample data was omitted from the linear regression because sample preparation itself was considered an additional variable. The goal of the linear regression was to observe the effect of one variable—thickness—on elongation. There were more data points of unpolished samples available, so these were used for the regression.

A linear trend between total elongation and thickness is stronger in Grade 2 than Grade 5 titanium, given by the R^2 values of 0.699 and 0.222, respectively. The R^2 of

Grade 2 is still not considered a strong enough value to reliably predict the total elongation at thicknesses outside the given range, but it does demonstrate that the linear trend better describes the relationship between total elongation and thickness in Grade 2. Linear regression was also performed on the elongation at UTS and post-necking elongation as functions of thickness. Figure 25 shows the regression coefficients as well as R^2 values for the trend lines.

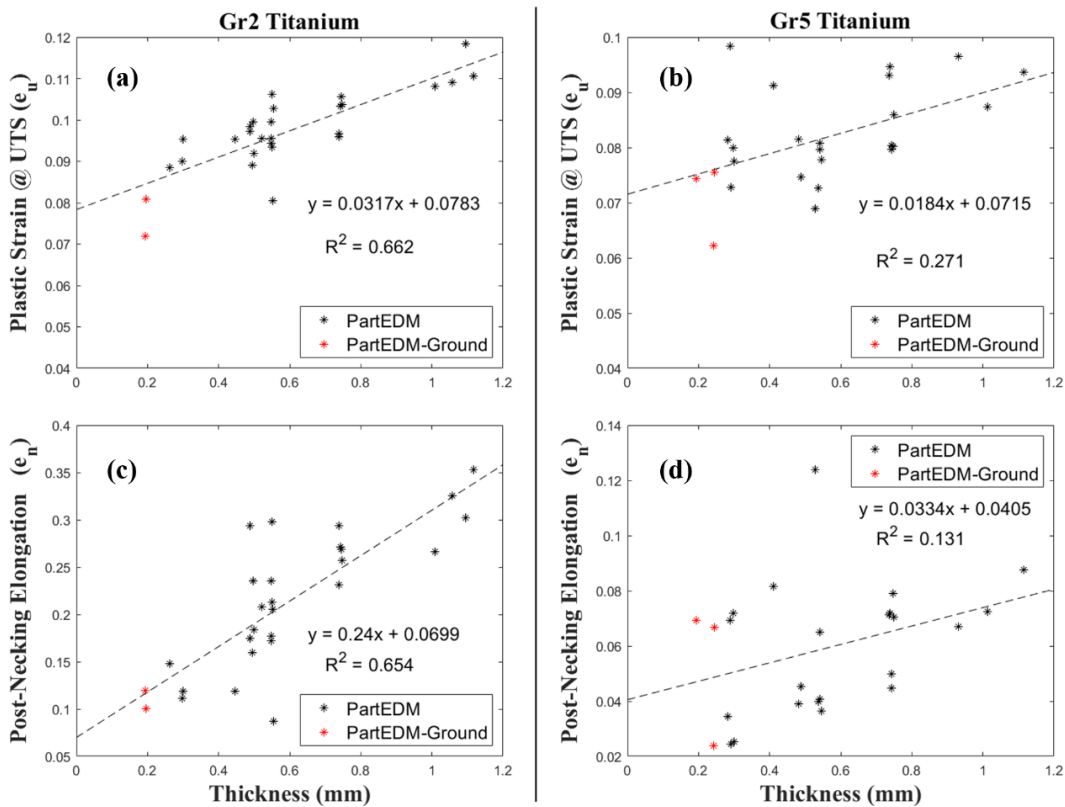


Figure 25: (a)(b) Plastic strain at UTS (e_u) vs. thickness for Grade 2 and Grade 5 titanium, respectively. (c)(d) Post-necking elongation (e_n) vs. thickness for Grade 2 and Grade 5 titanium, respectively.

The R^2 values for these linear trends are again stronger for Grade 2 than Grade 5. Furthermore, the R^2 values differ the most for the linear relationship between post-necking elongation and thickness, with values of 0.654 and 0.131 for Grade 2 and Grade 5, respectively.

P-values for a significance level (α) of 0.05 were calculated for the Pearson's correlation coefficient, R. The p-values are given in Table 4.

Table 4: P-values calculated for the Pearson's correlation coefficient in each case.

	P-values		
	e_t vs. t	e_t vs. t	e_n vs. t
Grade 2 Ti	< 0.05 (2.98×10^{-8})	< 0.05 ($1.92 \cdot 10^{-7}$)	< 0.05 ($1.92 \cdot 10^{-7}$)
Grade 5 Ti	< 0.05 (0.0175)	< 0.05 (0.00766)	> 0.05 (0.0751)

Using a significance level of 0.05, both materials show significant relationships between total elongation and thickness and elongation at UTS and thickness. However, the p-values of Grade 2 are much smaller than those of Grade 5, indicating a stronger likelihood that those elongation values are dependent on the thickness. Additionally, only Grade 2 shows a statistically significant linear relationship between post-necking elongation and thickness, while Grade 5 does not have a statistically significant relation of the same kind, given by the p-value of 0.0751. Therefore, the amount of post-necking elongation is dependent on thickness in Grade 2 titanium, while the post-necking elongation does not have the same thickness dependence in Grade 5.

Looking at the fracture surface of samples with similar thickness, as shown in Figure 26, it is apparent that Grade 5 samples experience less reduction in area and thereby less necking than Grade 2.

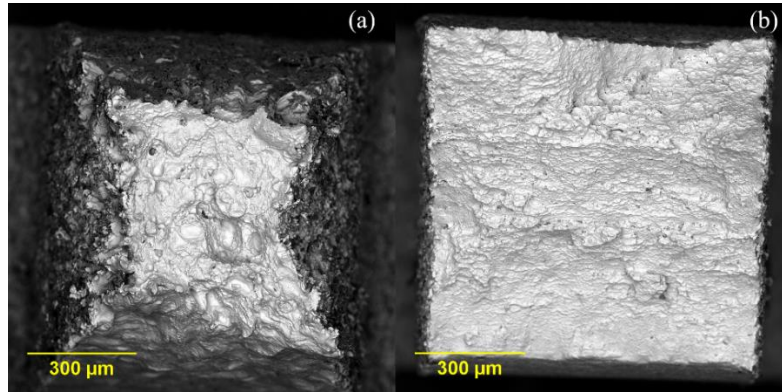


Figure 26: (a) Fracture surface of 1.118 mm thick Grade 2 sub-scale sample (b) Fracture surface of a 1.115 mm thick Grade 5 sub-scale sample.

Figure 27 also shows the comparison of a different set of Grade 5 and Grade 2 post-mortem samples to highlight the minimal necking in Grade 5.

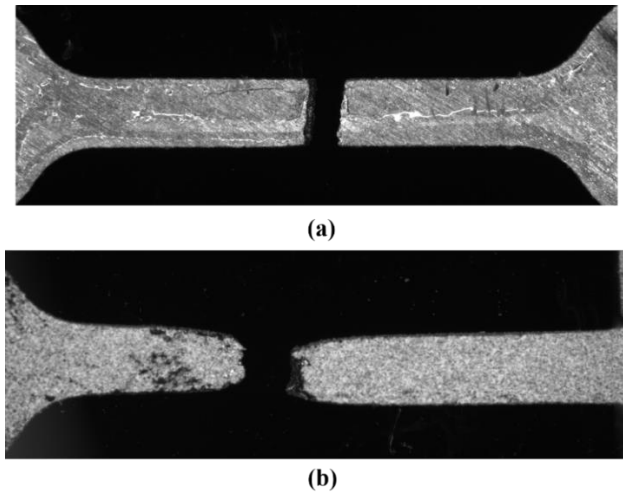


Figure 27: (a) Post-mortem Grade 5 sample, showing minimal necking (b) Post-mortem Grade 2 sample exhibiting significant necking.

The necking in the Grade 2 sample in Figure 27 (b) is apparent and stands in stark contrast to the Grade 5 sample which broke cleanly with little necking.

CHAPTER VI

CONCLUSIONS

Typically, the more ductile the material, the more it will neck. It is usually the ductility that makes a material more damage tolerant, and in this way Grade 2 is more damage tolerant than Grade 5 titanium. However, the tensile data reveals that the elongation of Grade 2 shows the stronger dependence on sample thickness, given by the much smaller p-values. The findings of this research are counterintuitive because they imply the more damage tolerant material is the most size-effect sensitive. However, it makes sense that the more damage tolerant, more ductile material should exhibit a greater size effect because the relative degree of necking is more severe in thinner samples. The time between the onset of necking and failure is faster in thin samples because there is less material to neck through. The mechanism responsible for damage tolerance—ductility—is also the mechanism behind the thickness effect. As a result, the more ductile material will not tolerate much deformation before failure in very thin samples. Put differently, the thinner the sample, the sooner the failure for damage tolerant (ductile) materials.

In this way, Grade 5 is not as damage tolerant and cannot sustain as much plastic deformation post-UTS as Grade 2 can. For this reason, Grade 5 does not exhibit a thickness dependence for post-necking elongation, and it will fail largely after the same amount of elongation regardless of thickness.

The UTS and YS data shows no indications of dependence on thickness for either grade of titanium, but there is notable scatter in the data, especially for Grade 5. The

techniques employed to improve the surface finish of the samples did not result in property values that deviated considerably from the unpolished samples. One possible reason for the lack of improvement could be that the polishing procedure was insufficient at removing a significant amount of stress concentrators from the EDM recast layer. Elongation plotted as a function of thickness did reveal signs of a linear correlation with sample thickness, most noticeably for Grade 2. P-values were calculated for the Pearson's correlation coefficients associated with the linear relationship between thickness and each of the three types of elongation (total elongation, elongation at UTS, and post-necking elongation). Using a significance level of 0.05, the total elongation and elongation at UTS were both shown to have statistically significant dependence on thickness for both materials. However, the p-values of Grade 2 were significantly smaller than those of Grade 5. Therefore, there is stronger evidence of an elongation-thickness dependency in Grade 2 titanium.

The p-value for the relationship between post-necking elongation and thickness in Grade 5, 0.0751, was larger than the significance level of 0.05. Therefore, the relationship is not statistically significant. This is in contrast with Grade 2, where the post-necking elongation does have a statistically significant linear dependence on thickness. The same range of thicknesses were tested for each material, yet only one exhibited a change in post-necking elongation as thickness was varied.

Two alternative methods for measuring the cross-sectional areas of the sub-scale tensile specimens were also developed, which are referred to as the optical method and the electrical resistance method. Using the alternative methods, a nearly 1:1 relationship

with the traditional method of using micrometers was determined, and there was little variance among the data. This suggests that the alternative methods are suitable replacements for using micrometers. These methods are especially useful for specific instances where micrometers are known to result in significant error (e.g., in situations where mass finishing or electro polishing are used to improve the surface finish of individual samples). Accurate area measurement is critical for sub-scale tensile testing because slight miscalculation has stronger impact on the calculated mechanical properties. The optical method is particularly helpful in situations where a non-contact method is preferred for preserving the surface finish of the sample.

Future Recommendations

In this investigation, 40 samples of each material were tensile tested. Regarding future work, ideally hundreds of sub-scale tensile samples should be tested to verify these findings. Only a third of the samples tested in this investigation were polished. In future work, additional polished samples should be tested so that statistical analysis can be conducted on them as well. Then, the p-values of the polished and unpolished samples could be compared to determine whether the degree of thickness dependence is affected by surface finish. Additionally, there were many variables in the employed polishing method that were not tightly controlled and measured, such as the pressure applied to the rotary tool during polishing and the duration of polishing on each surface. For future experiments, it is recommended that a more tightly controlled polishing procedure, such as mass finishing, is used to achieve both uniform finish across the individual sample surfaces and uniform finish across the entire batch of samples.

REFERENCES

- [1] S. Martel, “Micromechanical Devices,” in *Wiley Encyclopedia of Biomedical Engineering*, John Wiley & Sons, Inc., 2006, pp. 1–7.
- [2] J. R. Porter, R. Wheeler, and M. Velez, “In-Situ Tensile Deformation of Additively Manufactured Ti 6Al 4V,” *Microsc. Microanal.*, vol. 21, no. S3, pp. 95–96, 2015, doi: 10.1017/S1431927615001270.
- [3] A. S. Reddy and D. Srinivasan, “Small scale mechanical testing for additively manufactured (direct metal laser sintered) monolithic and hybrid test samples,” *Procedia Struct. Integr.*, vol. 14, pp. 449–466, 2019, doi: 10.1016/j.prostr.2019.05.055.
- [4] J. Dzugan, M. Sibr, P. Konopik, R. Prochazka, and M. Rund, “Mechanical properties determination of AM components,” *IOP Conf. Ser. Mater. Sci. Eng. Sci. Eng.*, vol. 179, no. 1, 2017, doi: 10.1088/1757-899X/179/1/012019.
- [5] B. L. Boyce *et al.*, “Extreme-Value Statistics Reveal Rare Failure-Critical Defects in Additive Manufacturing,” *Adv. Eng. Mater.*, 2017, doi: 10.1002/adem.201700102.
- [6] B. C. Salzbrenner *et al.*, “High-throughput stochastic tensile performance of additively manufactured stainless steel,” *J. Mater. Process. Technol.*, vol. 241, no. 505, pp. 1–12, Mar. 2016, doi: 10.1016/j.jmatprotec.2016.10.023.
- [7] H. Liu, Y. Shen, S. Yang, P. Zheng, and L. Zhang, “A comprehensive solution to miniaturized tensile testing: Specimen geometry optimization and extraction of constitutive behaviors using inverse FEM procedure,” *Fusion Eng. Des.*, vol. 121,

- pp. 188–197, 2017, doi: 10.1016/j.fusengdes.2017.07.016.
- [8] “ASTM Standard B348/B348M-19.” ASTM International, West Conshohocken, PA, p., 2019, [Online]. Available:
https://compass.astm.org/EDIT/html_annot.cgi?B348+19.
- [9] S. S. Brenner, “Tensile strength of whiskers,” *J. Appl. Phys.*, vol. 27, no. 12, pp. 1484–1491, 1956, doi: 10.1063/1.1722294.
- [10] D. Y. W. Yu and F. Spaepen, “The yield strength of thin copper films on Kapton,” *J. Appl. Phys.*, vol. 95, no. 6, pp. 2991–2997, 2004, doi: 10.1063/1.1644634.
- [11] R. W. Hertzberg, R. P. Vinci, and J. L. Hertzberg, *Deformation and Fracture Mechanics of Engineering Materials*, 5th ed. John Wiley & Sons, Inc., 2013.
- [12] T. A. Kals and R. Eckstein, “Miniaturization in sheet metal working,” *J. Mater. Process. Technol.*, vol. 103, no. 1, pp. 95–101, 2000, doi: 10.1016/S0924-0136(00)00391-5.
- [13] H. H. S. Miyazaki, H. Fujita, “Effect of Specimen Size on the Flow Stress of Rod,” vol. 13, no. c, pp. 4–6, 1979.
- [14] C. Wang, S. Xue, G. Chen, and P. Zhang, “Constitutive model based on dislocation density and ductile fracture of Monel 400 thin sheet under tension,” *Met. Mater. Int.*, vol. 23, no. 2, pp. 264–271, 2017, doi: 10.1007/s12540-017-6404-7.
- [15] L. V. Raulea, A. M. Goijaerts, L. E. Govaert, and F. P. T. Baaijens, “Size effects in the processing of thin metal sheets,” *J. Mater. Process. Technol.*, vol. 115, no. 1, pp. 44–48, 2001, doi: 10.1016/S0924-0136(01)00770-1.

- [16] Y. H. Zhao *et al.*, “Influence of specimen dimensions and strain measurement methods on tensile stress-strain curves,” *Mater. Sci. Eng. A*, vol. 525(1–2), no. 68–77, 2009, doi: 10.1016/j.msea.2009.06.031.
- [17] A. V. Sergueeva, J. Zhou, B. E. Meacham, and D. J. Branagan, “Gage length and sample size effect on measured properties during tensile testing,” *Mater. Sci. Eng. A*, vol. 526, pp. 79–83, 2009, doi: 10.1016/j.msea.2009.07.046.
- [18] B. Fotovvati, S. A. Etesami, and E. Asadi, “Process-property-geometry correlations for additively-manufactured Ti–6Al–4V sheets,” *Mater. Sci. Eng. A*, vol. 760, no. May, pp. 431–447, 2019, doi: 10.1016/j.msea.2019.06.020.
- [19] A. Rashid, “Additive Manufacturing Technologies,” in *CIRP Encyclopedia of Production Engineering*, 2nd ed., Berlin, Heidelberg: Springer Berlin Heidelberg, 2019, pp. 39–46.
- [20] D. Sher, “2019 Additive Manufacturing Market Outlook and Summary of Opportunities,” 2018.
- [21] E. O. Ezugwu and Z. M. Wang, “Titanium alloys and their machinability—a review,” *J. Mater. Process. Technol.*, vol. 68, no. 3, pp. 262–274, Aug. 1997, doi: 10.1016/S0924-0136(96)00030-1.
- [22] I. Buj-Corral, A. Tejo-Otero, and F. Fenollosa-Artés, “Development of am technologies for metals in the sector of medical implants,” *Metals (Basel)*, vol. 10, no. 5, pp. 1–30, 2020, doi: 10.3390/met10050686.
- [23] G. E. Lucas, “Review of small specimen test techniques for irradiation testing,” *Metall. Trans. A*, vol. 21, no. 4, pp. 1105–1119, 1990, doi: 10.1007/BF02656531.

- [24] H. S. Cho, R. Kasada, and A. Kimura, “Effects of neutron irradiation on the tensile properties of high-Cr oxide dispersion strengthened ferritic steels,” *J. Nucl. Mater.*, vol. 367-370 A, no. SPEC. ISS., pp. 239–243, 2007, doi: 10.1016/j.jnucmat.2007.03.140.
- [25] D. A. LaVan and W. N. Sharpe, “Tensile testing of microsamples,” *Exp. Mech.*, vol. 39, no. 3, pp. 210–216, 1999, doi: 10.1007/BF02323554.
- [26] D. S. Gianola and C. Eberl, “Micro- and nanoscale tensile testing of materials,” *Jom*, vol. 61, no. 3, pp. 24–35, 2009, doi: 10.1007/s11837-009-0037-3.
- [27] S. Karnati, I. Axelsen, F. F. Liou, and J. W. Newkirk, “Investigation of Tensile Properties of Bulk and SLM Fabricated 304L Stainless Steel Using Various Gage Length Specimens,” in *Solid Freeform Fabrication 2016: Proceedings of the 26th Annual International Solid Freeform Fabrication Symposium – An Additive Manufacturing Conference*, 2016, pp. 592–604, [Online]. Available: <https://pdfs.semanticscholar.org/bdc1/e58ef21808e25a97fcd351047b5c2c6802eb.pdf>.
- [28] ASTM E8, “ASTM E8/E8M standard test methods for tension testing of metallic materials 1,” *Annu. B. ASTM Stand.* 4, no. C, pp. 1–27, 2010, doi: 10.1520/E0008.
- [29] T. M. Mower, “Degradation of titanium 6Al-4V fatigue strength due to electrical discharge machining,” *Int. J. Fatigue*, vol. 64, pp. 84–96, 2014, doi: 10.1016/j.ijfatigue.2014.02.018.
- [30] G. Antaki and R. Gilada, “Design Basis Loads and Qualification,” in *Nuclear Power Plant Safety and Mechanical Integrity*, Elsevier Inc., 2015, pp. 27–102.

- [31] C. S. Yen and T. J. Dolan, "A critical review of the criteria for notch-sensitivity in fatigue of metals," *Univ. Illinois Bull.*, vol. 49, no. 53, p. 62, 1952.
- [32] J. Strasky, M. Janecek, and P. Hrcuba, "Electric Discharge Machining of Ti-6Al-4V Alloy for Biomedical Use," *WDS'11 Proc. Contrib. Pap.*, pp. 127–131, 2011.
- [33] G. Lütjering and J. C. Williams, *Titanium*, 2nd ed. Springer, 2007.
- [34] H. Bisaria and P. Shandilya, "Machining of Metal Matrix Composites by EDM and its Variants: A Review," no. January 2015, DAAAM International, 2015, pp. 267–282.
- [35] L. C. Moody, I. J. Powell, D. O. Lewis, M. C. Johnson, B. G. Butler, and J. D. Paramore, "Cross-sectional area measurement by optical and electrical resistance methods for subscale mechanical testing of near-net-shape titanium components," *Int. J. Refract. Met. Hard Mater.*, vol. 92, p. 105265, 2020, doi: 10.1016/j.ijrmhm.2020.105265.
- [36] H. Schreier, J.-J. Orteu, and M. A. Sutton, *Image Correlation for Shape, Motion and Deformation Measurements*. New York, NY: Springer US, 2009.
- [37] ASTM, "Tension Testing of Metallic Materials," *ASTM Int.*, 2016, doi: 10.1520/E0008_E0008M-16A.
- [38] F. Iaconis, R. Steindler, and G. Marinozzi, "Measurements of cross-sectional area of collagen structures (knee ligaments) by means of an optical method," *J. Biomech.*, vol. 20, pp. 1003–1010, 1987, doi: 10.1016/0021-9290(87)90330-7.
- [39] L. B. Valdest, "Resistivity Measurements on Germanium for Transistors," *Proc. IRE*, vol. 42, no. 2, pp. 420–427, 1954, [Online]. Available:

<http://lampx.tugraz.at/~hadley/sem/4pt/Resistivity.pdf>.

- [40] I. Miccoli, F. Edler, H. Pfnür, and C. Tegenkamp, “The 100th anniversary of the four-point probe technique: The role of probe geometries in isotropic and anisotropic systems,” *J. Phys. Condens. Matter*, vol. 27, no. 22, 2015, doi: 10.1088/0953-8984/27/22/223201.
- [41] N. Kipnis, “A Law of Physics in the Classroom: The Case of Ohm’s Law,” *Sci. Educ.*, vol. 18, pp. 349–382, 2009, doi: 10.1007/s11191-008-9142-x.
- [42] H. J. Kim, R. S. Jonathan, P. Yeonjoon, C. K. Glen, H. C. Sang, and N. Anita, “System to Measure Thermal Conductivity and Seebeck Coefficient for Thermoelectrics,” *NASA*. p. 31, 2012, doi: papers3://publication/uuid/AC9DD985-9089-44C0-8EF1-93F59D5020E9.
- [43] J. T. Milck, “Electrical Resistivity Data and Bibliography on Titanium and Titanium Alloys.” pp. 1–41, 1970.
- [44] R. J. Wasilewski, “Observations on Electrical Resistivity of Titanium,” *Trans. Metall. Soc. AIME*, vol. 224, pp. 3–6, 1962.

APPENDIX


	Titanium Metals Corporation 100 Titanium Way Toronto, OH, 43064 Telephone (740) 537-5694, Fax (740) 537-5653	Approved Certificate Page 3 of 4		
	CERT ID 18498DB-10 01-AUG-2018 16:34:13 GMT	SOLD TO CUSTOMER TIMET Service Center St. Louis 1250 Interstate Drive, Wentzville, MO 63385		
PURCHASE ORDER 20167146				
Chemistry Statements 1. Hydrogen values reported in PPM. Hydrogen determined by inert gas fusion per ASTM E1447. Carbon determined by combustion per ASTM E1941. Oxygen and Nitrogen determined by inert gas fusion per ASTM E1409. Henderson Melt: Metallics determined by Inductively Coupled Plasma-Atomic Emission Spectrometry (ICP-AES) per ASTM E2371. Morgantown Melt: Copper and Boron by atomic spectrometry (ingot only) and all other elements by x-ray fluorescence spectrometry. 2. Residual elements each less than 0.10% maximum, 0.40% maximum total. 3. Balance titanium.				
Mechanical Properties Unless otherwise noted, testing performed at Toronto Laboratory, 100 Titanium Way, Toronto, OH, 43064, USA				
RTT - Longitudinal (ASTM E 8) After Fracture Test Condition: [MILL] Annealed 1 Hour @ 1400°F, AC				
	0.2YS	U.T.S.	2inEL	R.A.
Sample ID	ksi	ksi	%	%
2S	132	143	15	27
3S	131	142	15	30
RTT - Transverse (ASTM E 8) After Fracture Test Condition: [MILL] Annealed 1 Hour @ 1400°F, AC				
	0.2YS	U.T.S.	2inEL	R.A.
Sample ID	ksi	ksi	%	%
2S	144	153	16	32
3S	146	155	16	32
<i>This test report shall not be reproduced except in full, without the written approval of TIMET. The intentional recording of false, fictitious, or fraudulent statements or entries on this certificate may be punished as a felony under federal law.</i>				
First in Titanium Worldwide				

Figure A. 1: Material certification for the wrought as-received Ti-6Al-4V

Titanium Processing Center
51513 Industrial Drive
New Baltimore, MI 48047

Material Test Report

Date: 8/2/2018

Purchase Order# AI-56959380
Sales Order # 324125
PO Line Item # 1

Company Name: McMaster Carr Supply Company
PO Box 5516
Chicago, IL 60680-5516

Grade: CP Titanium Grade 2

Specification: ASTM B 265 ASME SB 265 EN10204

Size: 1.000" X 2.000" X 12"

Heat #: 502EM-20141057

CHEMISTRY:	C	0.010	Al
	N	0.003	V
	O	0.140	Pd
	Fe	0.020	Mo
	H ₂	0.0010	Ni
			Ti Balance

MECHANICALS: Tensile: 425
Yield: 318
Elong: 30.5%

R/A:

Product Annealed: Yes

SIGNATURE: _____

The material purchased on this order has not knowingly been exposed or come into contact with mercury or mercury products while in the possession of TPC.

www.titaniumprocessingcenter.com

Figure A. 2: Material certification for the wrought as-received CP-Ti (Grade 2)